Limited Blue Carbon Potential of Intertidal Seagrass Meadows in the Wadden Sea – A Case Study in a Tidal Basin

Veronika Mohr[1], Corinna Schrum[1,2], Wenyan Zhang[1]

[1]Institute of Coastal Systems – Analysis and Modeling, Helmholtz-Zentrum Hereon, Geesthacht, Germany
[2]Center for Earth System Sustainability, Institute of Oceanography, Universität Hamburg, Hamburg, Germany
Correspondence to: Veronika Mohr (Veronika.Mohr@hereon.de)

Abstract.

Seagrass meadows are widely recognized as a key blue carbon ecosystem. However, their sequestration potential varies remarkably between species and regions. In the world's largest tidal flat system, the Wadden Sea, the highly dynamic hydro-morphological environment affects carbon cycling, making a quantitative analysis of the sequestration potential of intertidal seagrass meadows extremely challenging. To fill this gap, we applied a coupled hydro-eco-morphodynamic model which resolves dynamic changes of seagrass to estimate carbon fixation by primary production and carbon burial rates in a tidal basin of the Wadden Sea, the Sylt- Rømø Bay, as a case study. We further applied particle tracking to assess the fate of shed seagrass leaves.

Our results indicate that the seagrass meadows in the bay have a primary production of $895 \pm 465\ tC\ yr^{-1}$ (or $40.8 \pm 7.7\ gC\ m^{-2}\ yr^{-1}$). Approximately 24% ($9.8 \pm 1.6\ gC\ m^{-2}\ yr^{-1}$) of the annually carbon fixed by primary production is stored in the meadow sediments, with a major part originating from the below-ground biomass. Approximately 28 % of the seagrass biomass is exported from the meadows as flotsam, and about a fifth of that (~6% of the total biomass) is deposited in salt marshes. The remaining seagrass biomass (~48%) are either deposited as POC outside of the seagrass meadows, remineralized or grazed.

Overall, we estimate a burial rate of $10.1 \pm 1.5\ gC\ m^{-2}\ yr^{-1}$ (including both autochthonous and allochthonous carbon) within the seagrass meadows, which is lower than previous estimates for both the seagrass in the region and global averages. Our findings also show that the continuity of seagrass meadows is crucial for the mid-term (decennial), and likely also for the long-term (centennial or longer) storage of organic carbon in the sediment.

1 Introduction

Even though Blue Carbon Ecosystems cover a comparatively small area globally, their importance for carbon sequestration is disproportionally high compared to terrestrial ecosystems (Duarte et al., 2013; Macreadie et al., 2021; Mcleod et al., 2011). All marine and especially coastal ecosystems are counted as Blue Carbon Ecosystems, with the most prominent examples being mangroves, tidal marshes and seagrasses (Lovelock and Duarte, 2019).

Seagrasses store carbon in their biomass and in the sediments underneath. While the carbon storage in the biomass is on short (seasonal to several years; leaves) to intermediate (decadal to centennial; roots and rhizomes) time scales (Zou et al., 2021), the carbon sequestered in the seagrass sediment can be stored there for millennia (Dahl et al., 2024; Lo Iacono et al., 2008; Piñeiro-Juncal et al., 2025). Compared to surrounding bare sediments, seagrasses enhance carbon burial by trapping allochthonous carbon in their canopy in addition to autochthonous carbon (Mazarrasa et al., 2015; Oreska et al., 2018; Ward et al., 2025). The subsequent carbon storage in the sediments depends on the seagrass species and meadow connectivity, as well as on environmental factors such as sediment properties and hydrodynamic conditions (Dahl et al., 2016; Johannessen, 2022; Röhr et al., 2018; Schaefer et al., 2024). Generally, larger seagrass species with persistent growth in high spatial density have higher carbon stocks than smaller, more sparse species (Kennedy et al., 2022). A study in a subtidal *Zostera marina* meadow indicated that the persistence of seagrass patches appears to be the most important factor for long term (centennial and longer) carbon storage in the sediments (Schaefer et al., 2025). On the other hand, carbon storage in seagrass meadows can vary significantly at local scales (Prentice et al., 2020; Ricart et al., 2020; Schaefer et al., 2025). This complicates the extrapolation of carbon sequestration rates in seagrass meadows from local measurements to large-scale and global estimates (Kennedy et al., 2010) and necessitates process-understanding of the different processes involved in carbon cycling in a seagrass ecosystem.

While most studies on seagrass carbon focus on the amount of carbon stored inside the seagrass meadows, the fate of the seagrass detritus (dead leaf and root material) is also important for understanding the impact of seagrass on the larger-scale carbon cycle beyond the habitat. According to existing literature, less than half of leaf material is buried within the meadow of its origin and the rest is either remineralized, grazed or exported outside the meadow (Duarte and Krause-Jensen, 2017; Jacobs et al., 1981; Kennedy et al., 2010; Zou et al., 2021). The exported carbon may end up in neighbouring ecosystems or be transported to the open ocean (Chang et al., 2024; Krumhansl et al., 2015). Since seagrass leaves are buoyant (Weatherall et al., 2016) and decompose slowly (half-life of 141 ± 30 days) (Pan and Holmer, 2025; Trevathan-Tackett et al., 2020) they can be distributed over large areas before settling down and being potentially buried in the sediment (Chang et al., 2024; Duarte and Krause-Jensen, 2017).

Little is known on the organic carbon stock and the blue carbon potential in the Wadden sea (Koplin et al., 2025). An estimation of the carbon stock and carbon sequestration rate in the German Wadden Sea was made by Oppelt et al. (2024) based on observations of seagrass spatial coverage. They estimated that ~1.3 Mt of carbon are stored in the upper $1\ m$ of sediment of German Wadden Sea seagrass meadows and that these meadows sequester up to 9182 t of Carbon per year. Most of the carbon sequestration occurs in the Northern Wadden Sea, where the seagrass meadows cover approximately 16% of the intertidal flats (Kloepper et al., 2017). However, the estimation by Oppelt et al. (2024) was based on sequestration rates for seagrass measured in Scottland (Potouroglou, 2017) and Portugal (Martins et al., 2022). This may induce bias and subsequently large uncertainties when the rates are directly transferred to the Wadden Sea without considering the dependence of sequestration rate on regional conditions (Dahl et al., 2016; Prentice et al., 2020; Ricart et al., 2015, 2020; Röhr et al., 2018; Schaefer et al., 2024).

In this study, we seek to fill the gap in quantitative research of carbon sequestration potential of intertidal seagrass meadows in the Wadden Sea. We developed a dynamic seagrass growth model based on observations of seagrass properties and seasonal change in the Wadden Sea and integrated it into a 3-dimensional hydro-morphodynamic model. The coupled model was then applied to the Sylt-Rømø Bay in the northern Wadden Sea as a case study. Our model explicitly resolves the bio-physical interactions between seagrass and ambient hydro-morphodynamic environments, including production of particulate organic carbon (POC) in the seagrass meadows and subsequent deposition or transport by currents. We further considered the shedding of leaves and used a particle tracker to identify the spatial distribution of shed seagrass leaves biomass and their contribution to carbon burial in adjacent ecosystems such as salt marshes. Other processes related to seagrass carbon such as remineralization or grazing are included indirectly through loss terms, even though they are not modelled explicitly. Our results depict a comprehensive picture of source-to-sink carbon pathways at a basin scale associated with seagrass.

2 Study Area: Sylt-Rømø Bay

The Sylt-Rømø Bay is a semi-enclosed tidal basin in the northern Wadden Sea at the border of Germany and Denmark. The islands of Sylt and Rømø separate the bay from the North Sea, while passageways to the islands cut the basin off from the neighbouring basins to the north and south, leaving only a narrow inlet as connection to the North Sea. Large-scale diking during the 20th century reduced the intertidal area, steepened the tidal flats and increased tidal amplitude (Reise, 1998), effectively limiting the suitable habitat for intertidal seagrass.

The bay has an area of approximately $410\ km^2$ with intertidal flats occupying ~45% of the area (Konyssova et al., 2025). The average water depth is approximately $4\ m$, with a maximum depth of $37\ m$ in the tidal inlet. The sediments are predominantly sandy, with coarser material in deeper channels and finer fractions on intertidal flats. The mud content is generally <5% but can reach up to ~50% in shallow areas, particularly within and adjacent to seagrass meadows. Overall, the isolation of the bay led to relatively stable morphodynamics and low sediment input from the North Sea (Konyssova et al., 2025). The two barrier islands shelter the bay from wind and waves from the North Sea. The main drivers for hydro- and morphodynamics are the semi-diurnal tides, storm surges and local winds. The tidal currents reach up to $2\ m/s$ in the intertidal channels. The mean tidal amplitude is $1.7\ m$ (Konyssova et al., 2025). Several studies on hydrodynamics and sediment transport have been carried out in this basin (de Beer et al., 2005; Fofonova et al., 2019; Kappenberg et al., 1998; Konyssova et al., 2025; de la Vega et al., 2018; Mohr et al., 2025; Pejrup et al., 1997).

The bay has a longstanding seagrass population, which is dominated by the perennial and intertidal seagrass *Zostera noltei*, which are intermixed with intertidal, annual *Zostera marina* (Dolch et al., 2017). The seagrass meadows are located in the upper intertidal zone, preferentially along the leeside of the islands. In recent years, the core area of meadows (i.e. the area with coverage > 60%) remained relatively stable albeit with annual variations in the less dense (coverage between 20% and 60%) meadow area (Dolch et al., 2013).

The seagrass in the Wadden Sea is also featured by a strong annual growth cycle. After winter, shoot density is low and growth resumes in spring when conditions (e.g. light and temperature) become favourable. The meadows reach their maximum extent and shoot density in August. The growth of leaves slows down by the end of August, and massive grazing by migratory birds starts in September, leading to a strong decline in shoot density. The decline in shoot density continues throughout the winter, while most roots and rhizomes underground remain (Philippart, 1995; Vermaat and Verhagen, 1996).

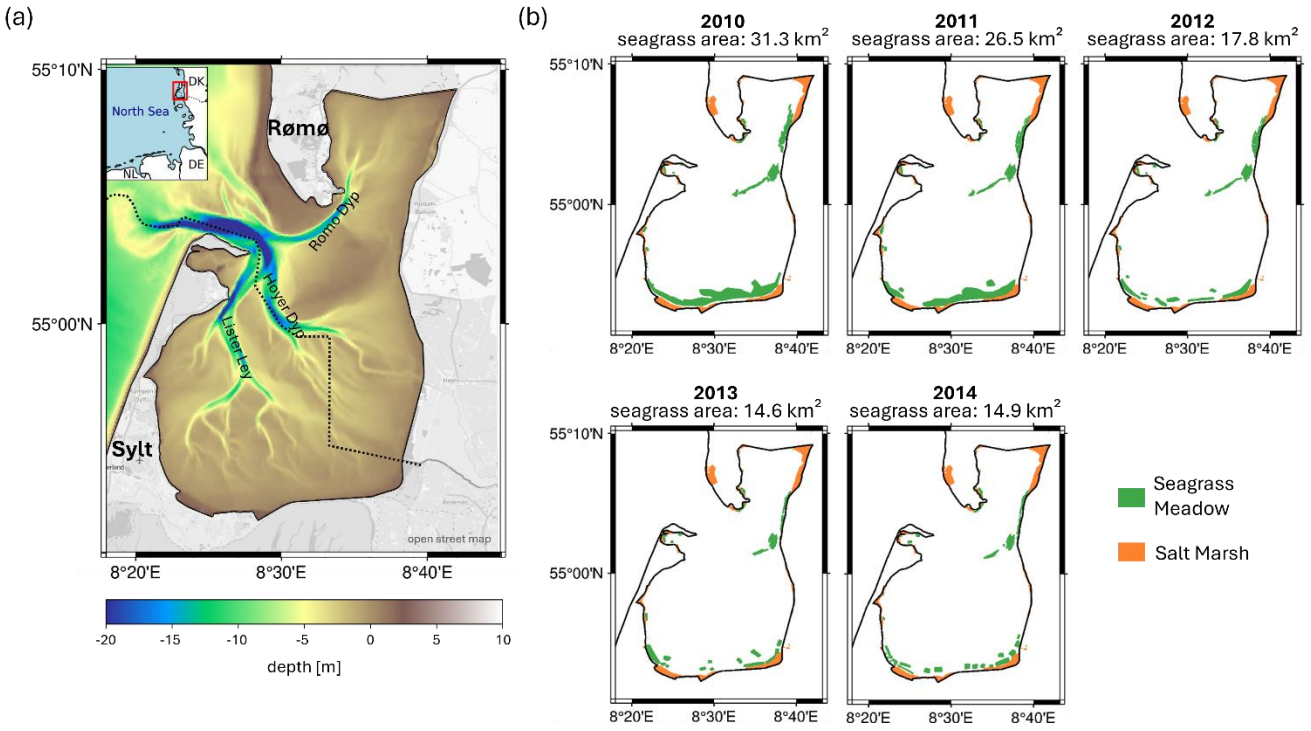

Figure 1: Map of the Sylt-Rømø Bay. (a) Topography of the bay. The grey dotted line is the border between Germany and Denmark. (b) Location of seagrass meadows and saltmarshes in in the Sylt-Rømø Bay from 2010-2014 from aerial surveys. The observational data for seagrass meadows can be accessed at LKN.SH Nationalparkverwaltung (2024) (German part), the data on the Danish part was provided by Lasse Ørsted Jensen (personal communication). The observational data for saltmarshes are provided at Datahuis Wadden (2023)

3 Methods

We implemented an iterative simulation procedure using the 3D-hydro- and morphodynamic model SCHISM (Zhang et al., 2016) and the intertidal seagrass growth model SGINT developed for this study. This iteration allows for a dynamic feedback between hydro- morphodynamics and seagrass.

The iteration is to run the hydro-morphodynamic model using an initial distribution of seagrass with prescribed shoot density, leaf biomass, and root biomass as the first step. After simulating one week of hydrodynamics and morphological changes, weekly mean values of temperature, inundation time, wind speed, and incoming solar radiation are calculated for each grid cell. These mean values are then transferred to the intertidal seagrass growth model SGINT to update the seagrass properties.

The map of seagrass properties is updated based on the simulation results from the seagrass model, which is used for the hydro-morphodynamic model to simulate seagrass-mediated currents and sediment dynamics for the next round (i.e. 7 days). Additionally, a fraction of the biomass that is lost between two successive timesteps of the SGINT model is converted to particulate organic carbon (POC) (see section 3.3). Subsequent transport, deposition and resuspension of the POC is simulated as a sediment class in the hydro-morphodynamic model. The iteration between the hydro-morphodynamic and the seagrass modelling continues until the end of the simulation period. The flowchart is illustrated in Figure 2.

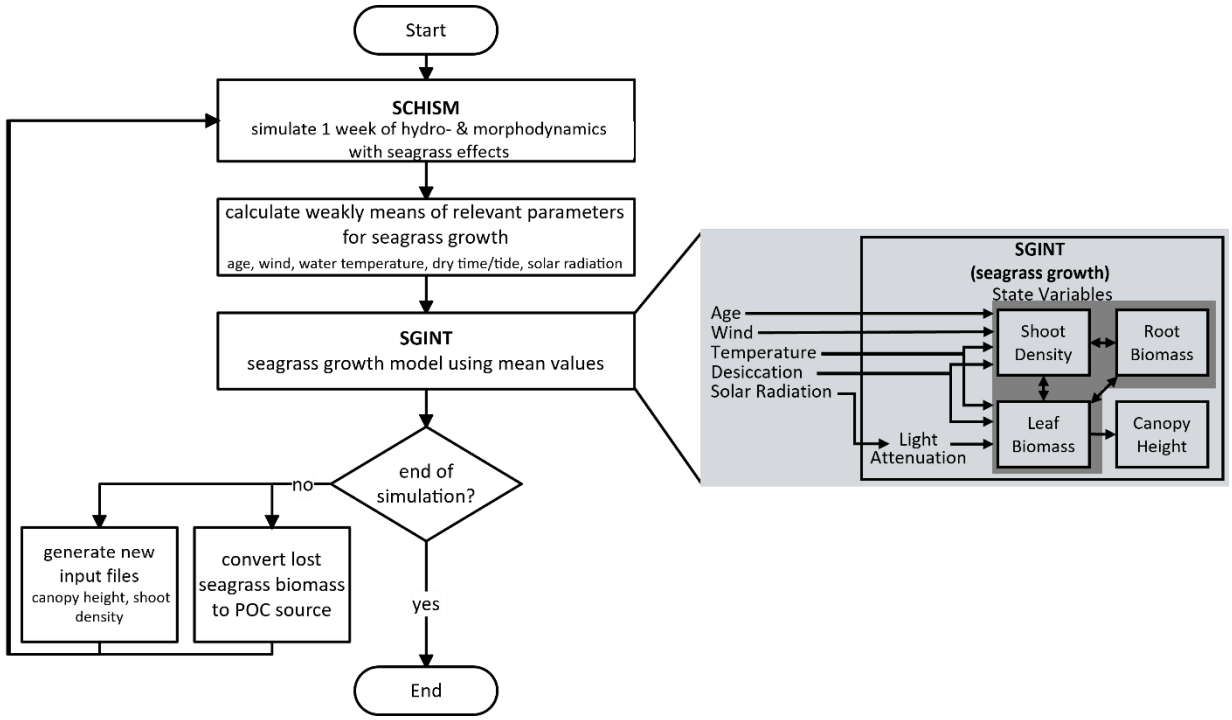

Figure 2: Flow chart of the modelling process, including a schematic overview of the intertidal seagrass model SGINT.

3.1 Hydro- and morphodynamical model

The numerical simulations of hydro- and morphodynamics were performed using the SCHISM model (Zhang et al., 2016), a 3D hydrodynamic model based on unstructured horizontal grids and hybrid s-z vertical coordinates. The model allows meter-scale spatial resolution with relatively large time steps due to its semi-implicit time-stepping scheme. SCHISM solves the baroclinic Reynolds-averaged Navier–Stokes equations under hydrostatic and Boussinesq assumptions, using a semi-implicit finite element/finite volume method with an Eulerian–Lagrangian approach. Tracer transport is simulated using a TVD scheme in the vertical and a WENO solver in the horizontal. Turbulence closure follows the generic length-scale formulation with k–ϵ parameterization (Umlauf and Burchard, 2005).

SCHISM includes MORSELFE (Pinto et al., 2012), a module for sediment transport, which accounts for morphological changes resulting from erosion and deposition.

The impact of vegetation such as seagrass on hydrodynamics is implemented through a modification of the momentum equation by introducing an additional drag term and by expanding the turbulent kinetic energy equation with an additional source of turbulence (Zhang et al., 2020). These additional terms depend on the vegetation properties including shoot density N, canopy height h_{can} and stem/leaf diameter D, as well as a vegetation-dependent drag term c_D, which are updated after every timestep of the seagrass growth model.

3.2 Seagrass Growth Model

The growth model for intertidal seagrass (SGINT) is developed based on the model for *Z. marina* from Zharova et al. (2001) and was adapted to the intertidal environments with several modifications to the growth and decline rates, as well as by parameter tuning to fit the observation data in our study area. The growth and decay of seagrass biomass depend on environmental parameters and internal feedback. The model uses three state variables, namely the single shoot biomass, the shoot density, and the below ground biomass. The canopy height is used as an auxiliary state parameter for computing the impact of vegetation on the hydro-morphodynamics. The growth or decay rate of the state variables is determined by temporally averaged values of temperature, radiation, mean inundation time, and wind speed. A detailed description of the SGINT model and its parameterization can be found in Appendix A.

3.3 Seagrass as a source of POC

The loss of seagrass biomass provides a source of POC, which is represented as a sediment-class tracer in the model. This allows for deposition and resuspension of the POC depending on the current velocity, direction and POC settling velocity. Seagrass biomass disintegrates into small particles due to decay and mechanical forces. For simplifying the model processes, we assume that the decay of seagrass biomass into POC occurs simultaneously with the loss of biomass at each model timestep and at the location where the seagrass biomass is lost.

Above-ground (AG) POC export is computed as:

$$POC_{AG} = \Delta B_{AG} \cdot f_{exp,AG} \tag{1}$$

where ΔB_{AG} $[kgC]$ is the change in AG biomass and $f_{exp,AG}$ is the fraction of the biomass exported from the meadow as POC. f_{exp} is based on global estimates of the portion of seagrass production exported from seagrass meadows as POC (Duarte and Krause-Jensen, 2017; Zou et al., 2021). The model continuously releases AG biomass POC to the water column where loss of seagrass biomass occurs.

Loss of below-ground (BG) biomass also produces POC. The produced BG biomass POC is added to the bottom sediments. It is worth noting that POC is considered as recalcitrant in this study, since seagrass decomposes slowly (Pan and Holmer, 2025; Trevathan-Tackett et al., 2020).

The burial rates of seagrass-originated POC depend strongly on the values set for f_{exp}, as illustrated by Figure B1. This study uses $f_{exp,AG} = 40\%$ and $f_{exp,BG} = 3\%$, based on globally combined observational values for seagrass (Duarte and Krause-Jensen, 2017; Zou et al., 2021), since no estimates exist for intertidal seagrass in the study region.

The burial rate of the seagrass- and non-seagrass-originated POC is calculated as the difference in POC stock in the active surface sediment layer between the initial and the final time step in the year. The resulting value refers to yearly carbon burial rate.

3.4 Tracking of seagrass debris

Loss of seagrass biomass in *Z. noltei* occurs when leaves are torn off either by wind, currents or during grazing. The resultant seagrass debris is transported by the currents and can be deposited on bare ground such as sand banks, beaches or in neighbouring salt marshes (Harwell and Orth, 2002; Hyndes et al., 2022; Mateo, 2010). To our knowledge, no research has been done yet on the fate of large seagrass debris in the Wadden Sea.

The possible trajectories of large seagrass debris being uprooted from the seagrass meadows are calculated using the lagrangian particle tracker OceanTracker (Vennell et al., 2021). OceanTracker uses the outputs of the hydrodynamic model to derive the physical conditions at the location of the particle and its subsequent trajectory. Particles representing seagrass leaves are released every 6 hours during the simulation at locations where loss of seagrass biomass occurs due to aging, wind scouring or shedding. The subsequent trajectories are calculated in two phases. The first phase is characterized by a positive buoyancy, since freshly torn-off seagrass leaves have a positive buoyancy and can therefore be transported over long distances (Berković et al., 2014; Harwell and Orth, 2002; Weatherall et al., 2016). After approximately three weeks, the drifting seagrass leaves start to lose their buoyancy due to decay (Berković et al., 2014). This turns to the second phase of the debris trajectories with a sinking velocity. The release of DOC or DIC due to decay is not incorporated in the model and the biomass of the particles does not change. We adopted a constant sinking velocity of 0.0076 ms^{-1} following the study by (Berković et al., 2014). Debris can strand and be deposited on the bottom, from where they can be resuspended when the critical friction velocity at the bottom exceeded 0.045 ms^{-1} (Berković et al., 2014). The final positions of the debris after 90 days in their second phase were analysed to estimate the distribution of the seagrass leaf debris biomass in the basin.

3.5 Model Setup

The model domain consists of the entire Sylt-Rømø Bay, as well as the adjoining part of the North Sea off the coasts of the islands of Sylt and Rømø. The grid resolution gradually increases from 500 m at the open boundary in the offshore area to 100 m inside the bay. In the vertical plane, a hybrid sz-grid is adopted, with 11 evenly distributed s-levels and one z-level. While the analysis mainly focuses on the bay, the offshore area plays a non-negligible role in providing both a sediment source and sink, and a buffer between the open boundary and the bay to mitigate potential boundary effects. The bathymetry was initialized with data from the digital terrain model obtained from the easyGSH-DB portal (Sievers et al., 2020). The water levels are

forced at the open boundary by a combination of short-term astronomical tides that are constructed using FES2014 (FES2014 Product [data set], 2023) and by long-term variations extracted from the Helgoland Tide Gauge which is located near the model boundary (Wasserstand (Ganglinie) Mess-Station Helgoland Binnenhafen [Data Set], 2024). Forcing data for temperature, solar radiation, and wind velocities are provided on an hourly basis by coastDat-3 (https://www.coastdat.de/).

The timestep of the hydrodynamic model is 2 minutes and the seagrass model is evoked every 7 days. Net relative leaf growth rate in *Z. notlii* typically ranges from $-0.05\ d^{-1}$ to $0.05\ d^{-1}$ (Philippart, 1995), implying relatively small changes in biomass over one week. Thus, the temporal update of seagrass properties every 7 days is sufficient to capture variability in temperature, light and inundation time, even though some short-term extreme events might not be fully captured. To figure out the uncertainty related to short-term extremes, shorter timesteps (1 day, 4 days) were tested but did not lead to a notable improvement in model performance while the computational cost increased considerably.

Three sediment classes are included in modelling, namely mud (grain diameter 50 µm), fine sand (grain diameter 120 µm), and coarse sand (grain diameter 300 µm). Additionally, three classes representing allochthonous and seagrass originated POC are included. The allochthonous POC is supplied from the offshore open boundary associated with primary production of phytoplankton, derived from ECOSMO simulation results (Daewel and Schrum, 2013). The parameter settings for the sediment classes can be found in Table 1. The sediment distribution was initialized using the interpolated grain size distribution dataset from AufMod (Sedimentologische Parameter Modellgitterpunkte (Projekt AufMod) [Data set], 2023). The model uses a single active surface sediment layer for calculation of erosion and deposition. The initial bed thickness is set to 10 m according to the thickness map of mobile sand produced by Zeiler et al. (2014). Validation of the hydro-morphodynamic model can be found in Appendix C and Mohr et al. (2025).

The seagrass model is parameterized to represent properties of the species *Z. noltei*, which is the dominant seagrass species in the study area. The less dominant *Z. marina* is excluded from the simulation, since it is unstable in space and time, as it is an annual variety that spreads via seed dispersal. A list of the parameters used for the seagrass model, as well as information on the tuning, can be found in the Appendix A. Seagrass growth, hydro- and morphodynamics are simulated for five years (2010-2014). The seagrass growth is restricted to the observed meadow areas to avoid model deviation (Fig. 1b).

The simulation period is 2010 – 2014. The hydro- and morphodynamics are modelled successively, while the seagrass model is reset at the beginning of each year to account for the changing extent of the seagrass meadows observed in the respective year. For the tracking of the seagrass debris released from the meadows in 2014, the first four months of 2015 were also modelled.

Table 1: List of model parameters for the different sediment classes: Grain diameter $\boldsymbol{d_{50}}$, settling velocity $\boldsymbol{w_{sett}}$, erosion rate $\boldsymbol{E_r}$ and critical shear stress for erosion $\boldsymbol{\tau_{cr}}$.

Sediment class	**Coarse sand**	**Fine sand**	**Mud**	**POC at open boundary**	**POC above ground biomass**	**POC below ground biomass**
$\boldsymbol{d_{50}}$ **[mm]**	0.3	0.12	0.05	0.05	2.0	1.0

w_{sett} [mm/s]	25	1	0.2	0.02	0.01	0.01
E_r [s/m]	3×10^{-5}	4.15×10^{-4}	8.15×10^{-4}	8.15×10^{-4}	8.15×10^{-4}	8.15×10^{-4}
τ_{cr} [Pa]	9.9	0.3	0.11	0.11	0.11	0.11

4 Results

4.1 Seasonal dynamics of Seagrass growth and primary production

The seasonal change of shoot biomass, shoot density and root biomass was validated against measurements of *Z. noltei* meadows located near Sylt, taken from six major meadows of different growth density from 2021-2023 (personal communication with Dr. Tobias Dolch). Since the observations are sparse in time and space, the observed values at multiple local sites covering several years were combined to get a monthly range of values for an annual cycle.

The simulated canopy height and shoot density are well within the range of the observed values (Fig. 3). The mean simulated canopy height has its minimum in April (Fig. 3a), and increases thereafter, reaching its maximum in late August. Afterwards, the canopy height declines, though a bit slower than the observations. The shoot density also has its minimum in April (Fig. 3b), and a strong growth of shoots starts from the beginning of June, being a few days later in the simulation than the observations. The shoot density reaches its maximum in September and afterwards declines.

Since there are no observations of root biomass in this region, the simulated root biomass was validated against a general seasonal trend that was observed in root biomass of seagrass meadows in the Netherlands (Philippart, 1995; Vermaat et al., 1987; Vermaat and Verhagen, 1996). The BG:AG ratio is approximately 2:1 in winter and 1:3 in summer. While the minimum and maximum of the BG biomass are in the same range as the observations, a time lag of about one month is seen in the simulation results in reproducing the maximum BG biomass (Fig. 3c).

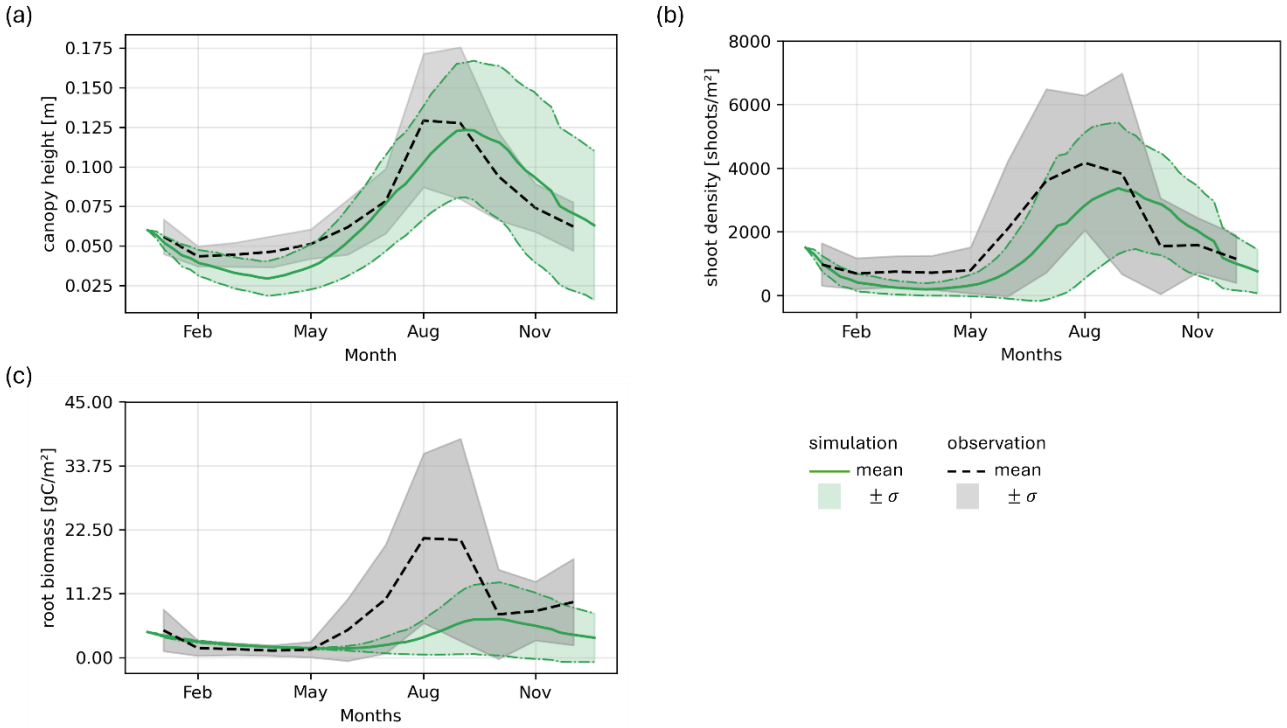

Figure 3: Comparison of observations and model results of (a) seagrass canopy height, (b) shoot density and (c) root biomass. The plots show the mean values and the range between ± standard deviation $\boldsymbol{\sigma}$. The model results are averaged over all computational cells with seagrass. The observation data of the root biomass are derived from the above ground biomass, using the ratio found in between above and below ground biomass in the Netherlands (Philippart, 1995; Vermaat et al., 1987; Vermaat and Verhagen, 1996).

The above ground biomass reaches a maximum of $16.8 \pm 5.4\ gC\ m^{-2}$ on average, which is approximately three times as high as the maximum of the below ground biomass ($5.7 \pm 1.5\ gC\ m^{-2}$) (Figure 4). The highest gain occurs in July ($2.8 \pm 0.7\ gC\ m^{-2}$) and the highest loss at the end of September ($2.7 \pm 0.7\ gC\ m^{-2}$).

Based on the validated growth dynamics, the annual primary production was estimated to be $850 \pm 425\ tC\ yr^{-1}$. This corresponds to a total annual primary production of $39.9 \pm 7.3\ gC\ m^{-2}\ yr^{-1}$ for the meadow area, of which $32.2 \pm 5.8\ gC\ m^{-2}\ yr^{-1}$ is above ground and $8.59 \pm 2.3\ gC\ m^{-2}\ yr^{-1}$ is below ground. The large variability stems from the differences in meadow area among the simulated years (see Figure 1b). Interannual differences in mean meadow biomass can also largely be explained by the different meadow extents, as the fraction of meadow area within the optimal depth range for growth (between -0.5 m and 0.5 m above the mean sea level) varies between years.

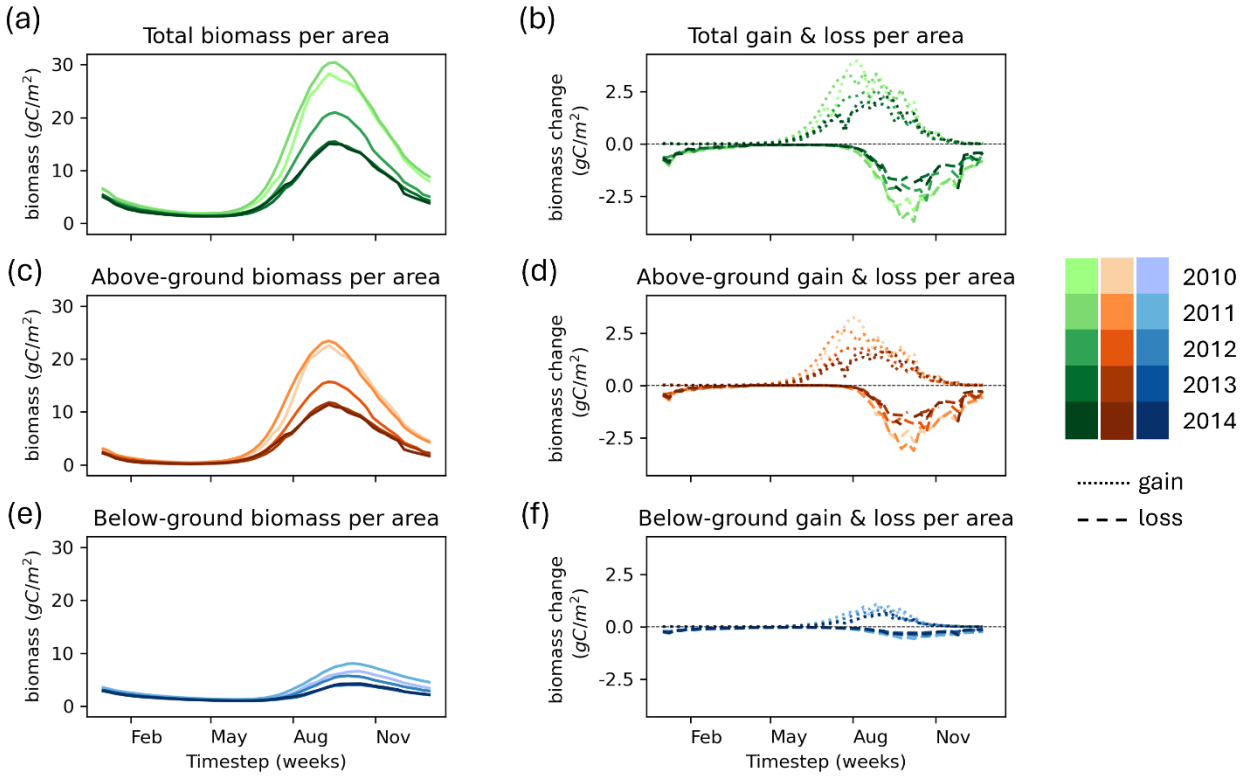

Figure 4: Development of (a) total, (c) above-ground, and (e) below-ground biomass and (b) total, (d) above ground, and (f) below-ground gain and loss of biomass throughout the year, for 2010 to 2014

4.2 Carbon burial caused by seagrass meadows

The carbon burial rate in the tidal flats was calculated as the difference in sedimentary carbon between the initial condition and the end of the simulation, divided by the number of simulated years. The areas with and without seagrass cover are distinguished. In addition, the areas with seagrass cover were categorized into several groups depending on the duration of seagrass cover in these areas in the 5-year period from the beginning of 2010 till the end of 2014.

Results show a remarkable variation of the average carbon burial rates among different areas (Fig. 5). In areas covered by seagrass, the burial rate of seagrass-originated POC increases linearly with the duration of seagrass cover (Fig. 5b-c). In areas persistently covered by seagrass meadows for all five years, the burial rate is $1.82 \pm 1.10\ gC\ m^{-2}\ yr^{-1}$ and $0.15 \pm 0.05\ gC\ m^{-2}\ yr^{-1}$ for the POC originating from above and below ground biomass, respectively. By contrast, in the intertidal areas without seagrass cover, the burial rate of seagrass-originated POC from above and below ground biomass is $0.10 \pm 0.16\ gC\ m^{-2}\ yr^{-1}$ and $0.001 \pm 0.004\ gC\ m^{-2} yr^{-1}$, respectively.

For allochthonous POC imported from the open boundary, its burial rate is highest on the tidal flats without any seagrass cover, but it also features a high spatial variability ($1.60 \pm 1.38\ gC\ m^{-2}\ yr^{-1}$). Its burial rate in areas with seagrass coverage is

lower, and especially among areas with seagrass coverage for one to four years, there are only minor changes in the burial rates (1 year: $0.39 \pm 0.38\ gC\ m^{-2}\ yr^{-1}$; 2 years: $0.33 \pm 0.35\ gC\ m^{-2}\ yr^{-1}$; 3 years: $0.43 \pm 0.53\ gC\ m^{-2}\ y^{-1}$; 4 years: $0.45 \pm 0.63\ gC\ m^{-2}\ yr^{-1}$, Fig. 5a). In the areas with a persistent seagrass cover for all five years, the burial rate of allochthonous POC is $0.73 \pm 0.65\ gC\ m^{-2}\ yr^{-1}$, remarkably higher than the areas with shorter duration of seagrass cover. However, although seagrass meadows are generally featured by a low burial rate of allochthonous POC, their presence can lead to an increase in burial rates. The longer the area is covered by seagrass, the stronger the effect becomes (Fig.5d).

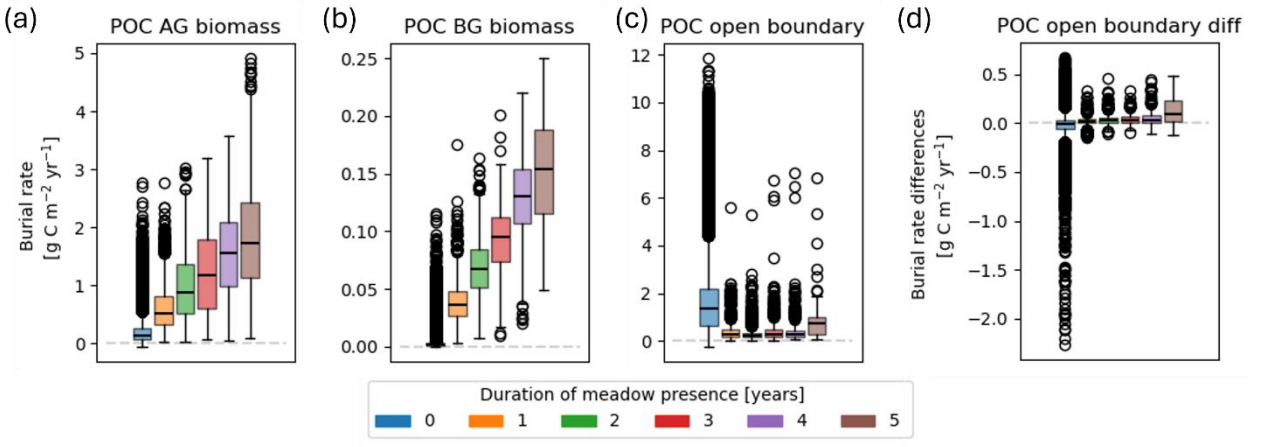

Figure 5: Boxplots of (a-c) annual burial rates on tidal flats for different POC sources, averaged over five years of simulation time and sorted by years with seagrass cover, and (d) difference in the annual burial rates compared to simulations without seagrass, for allochthonous POC from the open boundary. The boxplots show the median and quartiles for the burial rates on the model grid; dots denote outliers from the spread.

4.3 Fate of Leaf debris

Our simulation results show that approximately 28% of seagrass annual seagrass primary production is lost by primarily wind sloughing and subsequently transported away from the meadows by currents and wind in form of large debris. At the end of the tracking (114 days after release), 99.5% of the seagrass debris biomass is still located within in the basin. Their spatial distribution is shown in Fig. 6a. Almost half of the released debris biomass is located along the edges of the basin (49.9 ± 3.7 %), and the rest mostly on the tidal flats (44.4 ± 3.4 %). Only a small amount ends up in tidal channels (1.9 ± 0.2 %). While 70.7 ± 7.6 % of the debris biomass is produced and released in the southern half of the bay, only 48.5 ± 4.3 % of that ends up in the same part of the bay, while the rest 26.2 ± 5.4 % of the debris ends up in the north-eastern part of the tidal basin. It is worth noting that approximately 20.5 % of the released seagrass debris ends up in saltmarsh areas.

While the deposition of seagrass debris biomass at the edges and on the upper reaches of the tidal flats is consistent throughout the years, the debris biomass ending up adjacent to the channels and near the inlet can vary by more than 200% among the years (Fig. 6b), suggesting a dynamic depositional environment in these areas.

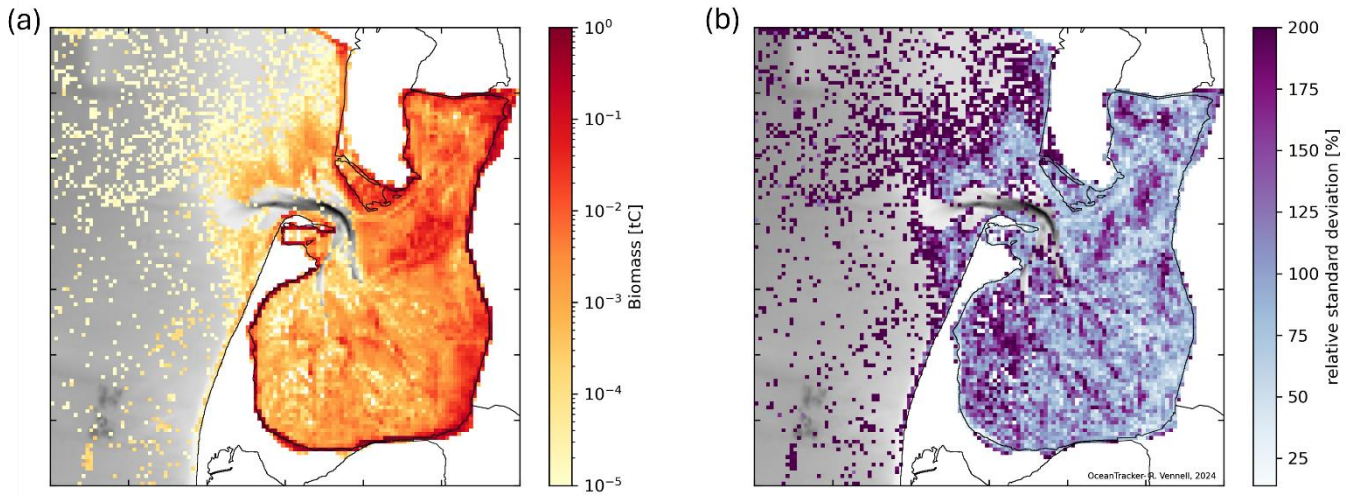

Figure 6: Distribution of seagrass debris biomass after 114 days since their release. Seagrass debris is released continuously at 6-hour intervals throughout the simulation at the locations where loss of seagrass biomass occurs for the respective timestep. a) shows the mean biomass distribution, averaged over five years for 2010-2014. The relative standard deviation b) shows the variability of the biomass distribution. The coastlines are from Sevdari and Marmullaku (2023).

5 Discussion

5.1 Carbon Pathways associated with seagrass

The carbon pathways associated with seagrass are summarized in Figure 7. In total, approximately $895 \pm 456\ tC\ yr^{-1}$ are taken up by seagrass primary production in the bay, with strong fluctuations among the years characterized by notable change in the spatial extent of seagrass meadows. This corresponds to a primary production of $40.8 \pm 7.7\ gC\ m^{-2}\ yr^{-1}$ inside the meadows.

Overall, 27.9 ± 4.6 % of the above ground seagrass biomass is torn out by wind and waves and redistributed inside the basin as large debris. Our modelling outcomes suggest that a fraction of the debris ends up in saltmarshes, amounting to 5.8 ± 1.4 % of the total annual seagrass primary production. This corresponds to a deposition of $3.7 \pm 2.4\ gC\ m^{-2}\ yr^{-1}$ of seagrass-originated carbon inside the saltmarshes when averaged over the saltmarsh area. Most of the remaining debris is redistributed inside the basin, with nearly half of it deposited at the basin edges and a majority of the other half deposited on the tidal flats after 114 days since the release. Only a very small portion (< 2%) ends up in the tidal channels or is further exported to the open North Sea.

The conversion of seagrass biomass to POC by decay and mechanical disintegration in our model depends strongly on the factor f_{exp} (see also Appendix B), which prescribes the fraction of lost biomass converted to POC at each timestep. Using values representative for global seagrass systems ($f_{exp,AG} = 40\%$ and $f_{exp,BG} = 3\%$) (Duarte and Krause-Jensen, 2017; Zou

et al., 2021), the model estimates that 26.1 ± 3.9 % of carbon by seagrass primary production is converted to POC. Uncertainty is introduced by applying the global values to the local system, the magnitude of which cannot be estimated due to a lack of observations. A fraction of this, 3.0 ± 0.6 % of the total seagrass-originated carbon, is buried in the seagrass sediments. This corresponds to an average carbon burial rate of $1.3 \pm 0.4\ gC\ m^{-2}\ yr^{-1}$ inside the seagrass meadows as POC. Approximately a third of the seagrass originating POC is deposited in the basin outside of seagrass meadows and 10.3 ± 3.1 % of the annual seagrass primary production ends up in the sediment in the basin outside the seagrass meadows, with a spatial averaged carbon burial rate of $0.2 \pm 0.04\ gC\ m^{-2}\ yr^{-1}$. The remaining 12.8 ± 5.1 % of seagrass-originated POC is either still suspended in the water column or transported out of the basin.

The majority of the below ground biomass $(100\% - f_{exp,BG})$ remains buried, indicating that 20.9 ± 2.1 % of the annul primary production is stored in the sediment beneath the meadows, corresponding to a burial rate of $8.5 \pm 1.4\ gC\ m^{-2}\ yr^{-2}$. Adding up the burial of seagrass POC and below ground biomass inside the meadows leads to a total burial rate of seagrass-originated carbon of $9.8 \pm 1.6\ gC\ m^{-2}\ yr^{-1}$, which amounts to 23.9 ± 2.2 % of the annual seagrass primary production in the bay. Even though the burial rate is lower, the fraction of seagrass primary production buried inside the meadows is higher than global estimates, which suggest that roughly 15 % of seagrass net primary production is buried in situ (Arias-Ortiz et al., 2026; Duarte and Cebrián, 1996). The burial rate increases slightly to $10.1 \pm 1.5\ gC\ m^{-2}yr^{-1}$ when the allochthonous POC from the open boundary is included in the calculation.

The fate of the remaining 25.1 ± 9.6 % of seagrass biomass is not resolved in detail in this study. It represents a loss term and can be attributed to grazing by migratory birds and chemical processes such as remineralization.

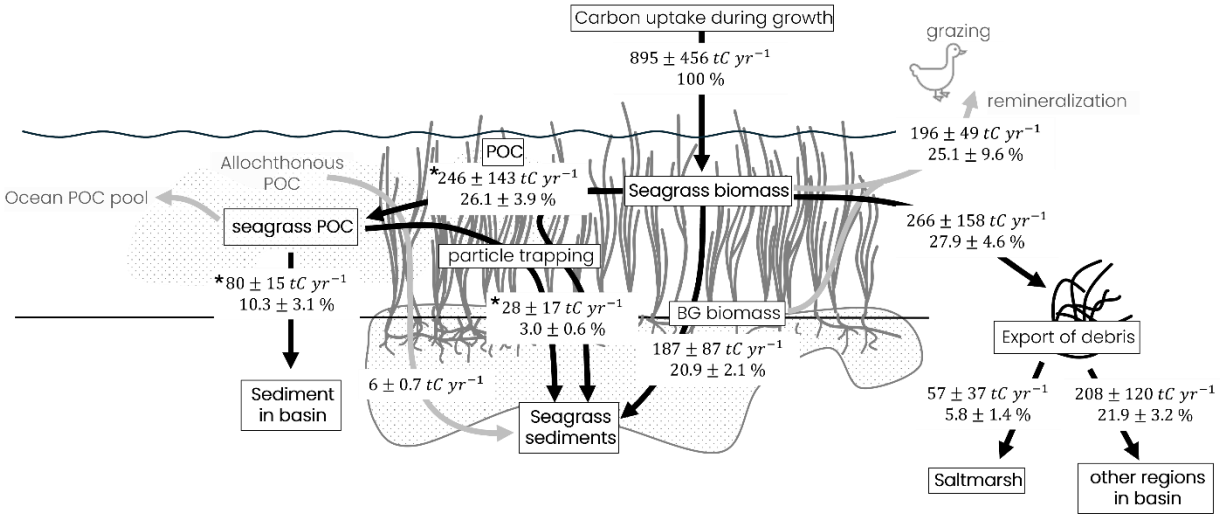

Figure 7: Conceptual figure of the carbon pathways of seagrass biomass in the basin. All values are annual values for the study area, averaged over the simulation period from 2010-2014. Values marked with * are dependent on the choice of f_{exp} for the conversion on lost biomass to POC. The percentages are relative to the total annual seagrass primary production (above and below ground). Paths drawn in light grey are not explicitly considered in the model or only considered partially. The area of the seagrass meadows from 2010-2014 is $20.3 \pm 6.3\ km^2$.

5.2 Carbon Sequestration in the Wadden Sea

The yearly carbon burial rate of $10.1 \pm 1.5\ gC\ m^{-2}\ yr^{-1}$ inside seagrass meadows obtained in this study is lower than estimates of long-term sequestration rates for the seagrass in the German Wadden Sea by other studies, which give sequestration rates of $24\ gC\ m^{-2}\ yr^{-1}$ (Mengis et al., 2022) and $44.45\ gC\ m^{-2}\ yr^{-1}$ (Oppelt et al., 2024). There are however several limitations for a direct comparison, including a mismatch of timescales. In addition, estimates from both existing studies are extrapolated based on data from other regions and seagrass species, which reduces their direct applicability for the meadows studied here. Sequestration rates are known to vary substantially among species (Duarte et al., 2010; Kennedy et al., 2022; Mazarrasa et al., 2015), among the same seagrass species in different regions (do Amaral Camara Lima et al., 2023; Greiner et al., 2016; Postlethwaite et al., 2018; Prentice et al., 2020) and even on local scales within a single meadow due to local environmental conditions or spatial and temporal continuity of the seagrass cover (do Amaral Camara Lima et al., 2023; Prentice et al., 2020; Schaefer et al., 2025). The unique hydrodynamic and morphodynamic conditions in the Wadden Sea, including constant and rapid morphological changes, and strong hydrodynamics by the tidal currents, also affect the carbon sequestration, which further limits the direct transfer of values from other regions.

Measurements of carbon content in and near seagrass meadows in the German Wadden Sea indicate slightly elevated carbon content in most meadows compared to nearby tidal flats, although the overall difference between seagrass and tidal flats were only marginally significant (Hommes, 2023; Schildt, 2025). Within meadows of comparable growth and sediment conditions, organic matter content correlates positively with seagrass biomass (Hommes, 2023). However, the variations were also correlated with changes in sediment dry bulk density (Schildt, 2025), which is one of the most important factors explaining variability in carbon content (Dahl et al., 2016; Röhr et al., 2016; Serrano et al., 2016). Therefore, it is not possible to distinguish whether the correlation is a result of seagrass presence, or if the regions where seagrass grows generally feature low hydrodynamics which lead to the deposition of fine-grained sediment and accordingly also carbon. The general observation that the presence of seagrass can be linked to higher carbon burial and therefore presumably also higher carbon content is however also reproduced by our model, indicating that seagrass plays a role in storing carbon in the sediment, provided that the cover is persistent for many years.

Based on the rates derived in this study, seagrass meadows in the Wadden Sea have a low burial rate especially compared to salt marshes, which are the major vegetated ecosystems in the Wadden Sea. Reported sequestration rates in salt marshes are substantially higher ($108 - 149\ gC\ m^{-2}\ yr^{-1}$) (Mueller et al., 2019; Oppelt et al., 2024). However, non-seagrass carbon is only partially included in this study and the actual burial rates in the seagrass meadows might be higher. The modelled input of seagrass biomass of $3.7 \pm 1.4\ gC\ m^{-2}\ yr^{-1}$ to the saltmarshes is only a fraction of their total sequestration rate. However, these values are spatial averages over the whole marsh area. Local contributions are likely higher at the edge of the marshes, where seagrass leaf material accumulates. Also, part of the seagrass leaves deposited on adjacent tidal flats in the model might also be transported into the salt marshes by wind, further increasing the contribution of seagrass biomass to the carbon burial in salt marsh sediments.

5.3 Carbon Sequestration in Seagrass Meadows worldwide

The range of sequestration rates in seagrass meadows worldwide found in literature is large, with some meadows acting as net carbon sinks and others as net sources (Alongi, 2018). However, most studies agree that seagrass is a net sink for carbon, either in their sediments or by transferring seagrass-bound carbon to other ecosystems (Alongi, 2018; Duarte et al., 2005; Kennedy et al., 2010; Mazarrasa et al., 2015). The mean carbon sequestration rates in global seagrass reported in literature also vary considerably, from $20\ gC\ m^{-2}\ yr^{-1}$ (Arias Ortiz, 2019) to more than $200\ gC\ m^{-2}\ yr^{-1}$ (Alongi, 2018). The consensus is however, that there are large variations in carbon sequestration capacity by seagrass (Alongi, 2018; Duarte et al., 2005; Kennedy et al., 2010; Mazarrasa et al., 2015) and that previous global calculations were overestimated (Lavery et al., 2013).
The carbon burial rates derived from our study are lower than the global average sequestration rates for seagrasses. This is in line with measurements in *Z. noltei* meadows in Portugal ranging from $15 - 122\ gC\ m^{-2}\ yr^{-1}$ (Martins et al., 2022), where carbon burial rates were reported to be negatively correlated to current velocities. In the highly dynamic environment of the Wadden Sea, we therefore expect values at the lower end of the range, as shown by the model results in our study.
In addition to the hydrodynamic conditions, the primary production obtained by our model ($40\ gC\ m^{-2}\ yr^{-1}$) is smaller than the primary production observed in *Z. noltei* meadows in the Netherlands and France ($115 - 184\ gC\ m^{-2}yr\hat{}-1$, (Pérez, 1989; Pérez-Lloréns and Niell, 1993; Vermaat et al., 1987)) and seagrass cover in the Wadden Sea exhibits a strong seasonality, with low or no cover during the most part of the year (November – June). Since the primary production limits the biomass that is available for burial in the sediments, this might be another reason why the carbon burial is comparatively low.

5.4 Limitations and future research needs

The burial rates calculated in this study are subject to several uncertainties related to both input data and model assumptions. A key source of uncertainty arises from limited empirical knowledge about seagrass detritus export from the meadows and the conversion of biomass to POC. In the current model, export of detritus and POC are treated separately, even though it is a continuous process and the exported detritus disintegrates further as it is transported. Additionally, available values for the disintegration of biomass to POC originate mainly from subtidal seagrass (Duarte and Krause-Jensen, 2017) but not from intertidal seagrass meadows due to lack of observation. This introduces uncertainties in our model and points out a need for field observations targeting export rates, decomposition, and remineralization processes in intertidal seagrass meadows Especially since there are no observations from the study region for POC burial rates in seagrass meadows or the export of POC and detritus, the values from this study remain a model estimation to be further confirmed by field measurements.
Another important limitation is the partial inclusion of allochthonous and autochthonous non-seagrass organic carbon. Organic carbon generated within the basin, such as phytoplankton, microalgal detritus, or resuspended particulate organic matter, is not included in the model due to lack of measurement data to constrain the model. These constituents can contribute significantly to the total organic carbon stock in seagrass meadows, and in many cases makes up more than 50% of organic carbon found in seagrass sediments (Oreska et al., 2018; Röhr et al., 2018; Ward et al., 2025), and similar observations were

made in Wadden Sea meadows (Schildt, 2025). Therefore, the carbon burial rates in this study likely underestimate the amount of carbon buried in seagrass meadows, as well as on the tidal flats. Although the meadows accumulate fine particulate matter during growing season, strong winter hydrodynamic conditions combined with seasonal leaf shedding typically lead to re-erosion of this material. As a result, much of the accumulated allochthonous POC is remobilized, limiting its long-term sequestration. Nonetheless, including additional non-seagrass organic carbon sources through tracer-based processes would improve the estimates of total carbon burial rates.

Another limitation of our model is that seagrass growth is only influenced by physical forcing and the effect of nutrients or competing organisms such as macro algae is not considered. Since the seagrass meadows in the Sylt-Rømø Bay have reached their largest extent in the recent decade and the population in the core areas appears stable, it can be assumed that the influence of non-physical factors is minor in this region and can reasonably be excluded from this study.

Since the influence of the seagrass on the currents and sediment transport plays a major role in the calculation of the burial rate of POC, uncertainties in the model results regarding bio-physical interactions between seagrass and hydro-morphodynamics also affect the overall assessment. For example, bending of the leaves is not considered in the model. In the intertidal zone, seagrass leaves most often lie flat on the seabed, and the currents skim over the canopy during low tides. Such bending of seagrass can have effects on the water flow in and above the canopy, and consequently on the self-shading by the plants and their ability to stabilize the sediment (Fonseca et al., 1982). A first-order approach using rigid cylinders was used to represent the effect of seagrass leaves on water flow (Zhang et al., 2020), and the uncertainty related to bending effects is not assessed in our study.

Further, wind-generated waves can have a considerable effect on seagrass and sediment on the coast, especially during storm events (Lettmann et al., 2009). Strong waves can lead to uprooting of seagrass plants, as well as affect the morphological processes and therefore also the burial of carbon in the sediments. However, under typical (non-storm) conditions, wind-wave-induced sediment erosion accounts only for a small portion of the overall erosion (Lettmann et al., 2009). Nevertheless, neglecting the influence of wind-waves might lead to an overestimation of carbon sequestration inside seagrass meadows and on the tidal flat in general.

6 Conclusions

Overall, our model results indicate that seagrass meadows in the Wadden Sea exhibit comparatively low carbon burial rates relative to both global averages and other ecosystems in the Wadden Sea. According to our estimations, annual seagrass primary production is approximately $895 \pm 456\ tC\ yr^{-1}$ for the entire bay, corresponding to $40.8 \pm 7.7\ gC\ m^{-2}\ yr^{-1}$ inside meadows. The modelled carbon burial rate per area of meadows is $10.1 \pm 1.5\ gC\ m^{-2}\ yr^{-1}$, which is significantly lower than previous estimates for the region.

The majority of seagrass-originated carbon buried into the seagrass sediments originates from the BG biomass. Approximately 20.9 ± 2.1 % of the total annual primary production remains buried in the sediments from the BG biomass. In addition, POC

formed by decay and mechanical forces from the AG and BG biomass contributes to the seagrass-originated carbon in the seagrass sediments. Approximately 3.0 ± 0.6 % of the total annual primary production of the seagrass is retained in the sediments as POC. In total, 23.9 ± 2.2 % of the primary production are buried in the sediment by the dead BG biomass and seagrass POC. The multi-year burial rates depend strongly on the continuity of the seagrass cover, with highest rate in areas persistently covered by seagrass. This indicates that also the long-term carbon sequestration is dependent on the continuity of the seagrass cover.

Approximately 28 % of the above-ground biomass is torn off by wind and currents annually and thereupon redistributed inside the basin in the form of large debris. Most of the debris stays inside the bay and is deposited on the shore or on the tidal flats. Roughly 5.8 ± 1.4 % of the total seagrass primary production is delivered to salt marshes, equating to $3.7 \pm 2.4\ gC\ m^{-2}\ yr^{-1}$ averaged over the marsh areas. This transfer underscores the importance of cross-habitat carbon exchange, with adjacent ecosystems playing an important role for the overall carbon storage in the system.

In summary, seagrass meadows in the Wadden Sea contribute to carbon burial, though their contribution is minor, especially compared to salt marshes. Nevertheless, more quantitative studies on the carbon burial rate and its spatial heterology inside seagrass meadows and also on the longer-term fate of seagrass biomass are necessary to better understand the carbon cycle of the system.

Appendix A - Description of the seagrass model

The seagrass model uses three state variables, namely the single shoot biomass $B_S\ [gC]$, below ground biomass $B_R\ [gC\ m^{-2}]$, and shoot density $N\ [shoots\ per\ m^2]$. Additionally, two auxiliary state variables are used, the total above ground biomass $B_{AG} = B_S * N\ [gC\ m^{-2}]$ and the canopy height $h_{can} = B_S * a_{ch}\ [m]$, where a_{ch} is a conversion factor from the biomass to the canopy height. The value for $a_{ch} = 20\ m\ gC^{-1}$ is based on measurements of biomass and canopy height in *Z. noltei* meadows (Laugier et al., 1999; Schanz and Asmus, 2003).

The changes to the single shoot biomass are represented as:

$$\frac{\boldsymbol{dB_S}}{\boldsymbol{dt}} = \left(\boldsymbol{Grow_S \cdot f_{il}(I,T) \cdot f_{tphot}(T) \cdot f_{Slim}(B_s)}\right) - \left(\boldsymbol{Loss_S \cdot f_{tloss}(T) \cdot f_{dry}(t_{dry}) \cdot f_{age}(d)}\right), \qquad (\boldsymbol{A}1)$$

where $Grow_S$ is the maximum growth rate for a single shoot, which is limited by light availability I, temperature T, and the biomass itself. Additionally, a fraction k_{rs} of photosynthetic growth is routed to the below ground biomass. $Loss_S$ is the single shoot mortality rate, which is influenced by temperature, inundation time t_{dry} and the phase of the growth cycle, represented as a function of the day of the year d. The limitation by light availability is calculated as

$$\boldsymbol{f_{il}} = \begin{cases} \boldsymbol{0}, & \boldsymbol{if\ I \le I_c} \\ \boldsymbol{\dfrac{I - I_c}{I_k - I_c}}, & \boldsymbol{if\ I_c < I < I_k}, \\ \boldsymbol{1}, & \boldsymbol{if\ I_k \le I} \end{cases} \qquad \boldsymbol{I_c = I_{c20}\theta_{Ic}^{(T-20)}}, \qquad \boldsymbol{I_k = I_{k20}\theta_{Ik}^{(T-20)}} \qquad (\boldsymbol{A}2)$$

where I is the radiation at the top of the canopy, I_c is the compensation irradiance, I_k the saturation irradiance, I_{c20} and I_{k20} the compensation and saturation irradiance at 20°C, respectively, θ_{Ic} and θ_{Ik} the temperature coefficients, and T the temperature.

The temperature dependency of photosynthetic growth is described as a bell-shaped function (Voinov and Akhremenkov, 1990)

$$\boldsymbol{f_{tphot}} = \begin{cases} \boldsymbol{k_0}^{\left((\boldsymbol{T_{opt}}-\boldsymbol{T})/\boldsymbol{T_{opt}}\right)^{\boldsymbol{st}}}, & \boldsymbol{if\ T \le T_{opt}} \\ \boldsymbol{k_m}^{\left((\boldsymbol{T}-\boldsymbol{T_{opt}})/(\boldsymbol{T_{max}}-\boldsymbol{Topt})\right)^{\boldsymbol{st}}}, & \boldsymbol{if\ T > T_{opt}} \end{cases} \quad (\boldsymbol{A}3)$$

where T_{opt} is the optimal temperature, T_{max} is the maximum temperature, k_0 and k_m are the function values at $T = 0$ and $T = T_{max}$, and st is the controlled shape of the function.

Additionally, the single shoot biomass is limited by the maximum leaf length

$$\boldsymbol{f_{Slim}} = \begin{cases} \boldsymbol{1} - (\boldsymbol{B_s}/\boldsymbol{\sigma_S})^{\boldsymbol{2}}, & \boldsymbol{if\ S \le \sigma_S} \\ \boldsymbol{0}, & \boldsymbol{if\ S > \sigma_S} \end{cases}, \quad (\boldsymbol{A}4)$$

where σ_S is the corresponding single shoot biomass for the maximum leaf length that a single shoot can reach.

Loss of seagrass biomass is caused by mortality and respiration, enhanced by desiccation, bird grazing, sloughing by wind and aging (Azevedo et al., 2017; Suykerbuyk et al., 2018). The mortality rate of intertidal seagrass increases with temperature (Massa et al., 2009), which is represented in the limiting function by temperature

$$\boldsymbol{f_{tloss}} = \boldsymbol{\theta_{loss}}^{(\boldsymbol{T}-\boldsymbol{20})}, \quad (\boldsymbol{A}5)$$

where θ_{loss} is the temperature coefficient.

The function for increased mortality due to desiccation is based on the mortality function by Voinov and Akhremenkov (1990)

$$\boldsymbol{f_{dry}} = \begin{cases} \boldsymbol{1} + \boldsymbol{\alpha}\left(\boldsymbol{t_{dry,min}} - \boldsymbol{t_{dry}}\right)^{\boldsymbol{2}}, & \boldsymbol{if\ t_{dry} < t_{dry,min}} \\ \boldsymbol{1}, & \boldsymbol{if\ t_{dry,min} \le t_{dry} \le t_{dry,max}} \\ \boldsymbol{1} + \boldsymbol{\beta}\left(\boldsymbol{t_{dry}} - \boldsymbol{t_{dry,max}}\right), & \boldsymbol{if\ t_{dry} > t_{dry,max}} \end{cases} \quad (\boldsymbol{A}6)$$

where t_{dry} is the mean inundation period per tidal cycle, $t_{dry,min}$ the lower limit for seagrass growth and $t_{dry,max}$ the upper limit for seagrass growth. α and β are rate coefficients for the shape of the function.

Wind sloughing increases the mortality. The function is based on Plus et al. (2003)

$$\boldsymbol{f_{wind}} = \boldsymbol{1} + \left(\boldsymbol{r_{lmw}} \cdot \boldsymbol{v_{wind}}\right), \quad (\boldsymbol{A7})$$

where r_{lmw} is the leaf mortality coefficient due to wind and v_{wind} is the depth integrated wind impact.

Since the growth and decline of seagrass in the Wadden Sea follow an annual cycle, a general estimation of the age of above-ground seagrass can be made based on the season. At the beginning of the growth season, the mortality is low and then continuously increases towards autumn, before it drops again toward the beginning of the growth season. This loss function also represents other seasonal loss terms not related to the age of the above-ground seagrass. A major contributor to this

seasonal increase in loss is the grazing in autumn when the Wadden Sea serves as a key stop for millions of migratory birds (Jacobs et al., 1981). This is represented in the limiting function

$$f_{age} = 0.5 \cdot tanh\left(\frac{\left((d - d_{grow})\%366\right) - (d_{loss} - d_{grow})}{r_{dloss}}\right) + 0.5, \quad \textbf{(A8)}$$

where d is the day of the year, d_{grow} is related to the start of the growth season, d_{loss} is related to the beginning of the major seagrass loss. Both d_{grow} and d_{loss} are specified as day of the year. r_{dloss} is a rate related to the steepness of the function.

The changes to the number of shoots per m² are calculated as

$$\frac{dN}{dt} = \left(Grow_N \cdot f_{il}(T, I) \cdot f_{tprod}(T) \cdot f_{AGlim}(B_{AG}) \cdot f_{Rlim}(B_R)\right) - \left(Loss_N \cdot f_{tdry}(t_{dry}) \cdot f_{age}(d) \cdot f_{wind}(w)\right), \quad \textbf{(A9)}$$

where $Grow_N$ is the shoot recruitment rate and $Loss_N$ the shoot loss rate. It is assumed that the growth of shoots depends on the growth conditions of the above ground biomass (Zharova et al., 2001), therefore f_{tprod} has the same shape as f_{tphot}.

In addition, the appearance of new shoots is space limited by the above ground biomass and growth limited by the available root biomass

$$f_{AGlim} = \begin{cases} 1 - (B_{AG}/\sigma_{AG})^2, & if\ B_{AG} \le \sigma_{AG} \\ 0, & if\ B_{AG} > \sigma_{AG} \end{cases} \quad \textbf{(A10)}$$

where σ_{AG} is the above ground biomass above which no new shoots are produced and

$$f_{Rlim} = \frac{B_R}{B_R + \epsilon}, \quad \textbf{(A11)}$$

where ϵ is the half-saturated constant for above ground biomass.

Changes to the root biomass are calculated as the sum of three different parts: the growth of the roots, which is rerouted from the leaf growth, the loss due to mortality and the loss of biomass due to uprooting. The resulting change of the root biomass is calculated by

$$\frac{B_R}{dt} = k_{rs} \cdot Grow_s \cdot f_{il}(I) \cdot f_{tphot}(T) \cdot B_{AG} - Loss_R \cdot B_R - Loss_N \cdot f_{age}(d) \cdot f_{tdry}(t_{dry}) \cdot B_{upr} \cdot N, \quad \textbf{(A12)}$$

where k_{rs} is the fraction of above ground growth rerouted to the roots, and B_{upr} the below ground biomass lost due to uprooting of a single shoot.

A sensitivity analysis was carried out to test how different parameters impact the seagrass growth. As definitive values were not available from literature for the Wadden Sea for all of the different parameters affecting the growth of the *Z. noltei*, the values used as a base for tuning are additionally based on values either reported for *Z. noltei* from different regions, mainly from the Mediterranean and southern France (Kombiadou et al., 2014; Laugier et al., 1999; Peralta et al., 2000, 2002; Plus et al., 2003) or values reported for *Z. marina* (Abe et al., 2003; Bach, 1993; Dennison and Alberte, 1982; Olesen and Sand-Jensen, 1993; Rasmussen, 1973; Verhagen and Nienhuis, 1983). An overview of the parameters used for tuning can be found in Table A1.

Table A1: List of parameters used in the model and the ranges used during the sensitivity tests. Whenever possible, values for *Z. noltei* were used as reference. In cases where no values for *Z. noltei* were available, or only available for different regions, values for *Z. marina* were also included. The values for *Z. marina* are marked with *. Since no values are available for the maximum above ground biomass above which no new shoots are produced, the values referenced are the maximum above ground biomass observed. These values are marked with **.

Parameter	Long name	Range	Sources	Param test scope	Value used in study	Unit
I_{k20}	saturation irradiance	~20-200 ~22 * ~ 88 * ~70 ~400	Kohlmeier (2016) Dennison and Alberte (1982) Abe et al. (2003) Peralta et al. (2002) Leuschner and Rees (1993)	20 - 200	120	W/m²
I_{c20}	Compensation irradiance	~2 * ~2.5 (20°C) * ~4 (15°C)- 10 (21°C) * ~1.2 ~4.6 ~12-15 ~1.3	Dennison and Alberte (1982) Abe et al. (2003) Olesen and Sand-Jensen (1993) Peralta et al. (2000) Peralta et al. (2002) Vermaat and Verhagen (1996)	1 – 15	9	W/m²
$T_{opt,ph}$	Optimal temperature for growth	23 * 10-15 * 25-30 * 25 * 25 * 20	Zharova et al. (2001) Rasmussen (1973) Marsh et al. (1986) Zimmermann et al. (1987) Pérez-Lloréns and Niell (1993) Leuschner and Rees (1993)	10 – 25	16	°C
$T_{max,ph}$	Maximum temperature for growth	37 20 * 30 *	Massa et al. (2009) Rasmussen (1973) Marsh et al. (1986))	20 – 32	29	°C
$Grow_S$	Maximum relative leaf growth rate	0.095 * 0.008 * 0.043 * 0.034 0.06	Bach (1993) Verhagen and Nienhuis (1983) Zharova et al. (2001) Plus et al. (2003) Vermaat et al. (1987)	0.01 - 0.09	0.016	-
$Loss_S$	Maximum relative Leaf mortality	0.05	Vermaat et al. (1987)	0.01 - 0.09	0.009	-
σ_S	Maximum single leaf biomass	0.0083 0.036 0.00047 *	Plus et al. (2001) Laugier et al. (1999) Vermaat and Verhagen (1996)	0.005 - 0.02	0.0125	gC/leaf
$Grow_N$	Maximum relative recruitment rate	0.05	Laugier et al. (1999)	0.01- 0.09	0.04	-
$T_{opt,pr}$	Optimal temperature for recruitment	10-15 *	Rasmussen (1973)	10 – 25 °C	18	°C

$T_{max,pr}$	Maximum temperature for recruitment	20 *	Rasmussen (1973)	20 – 32 °C	20	°C
σ_{AG}	Above ground biomass above which no new shoots are produced	50 * 82 ** 30 ** 15 ** 25 ** 49 ** 73 **	Zharova et al. (2001), based on Verhagen and Nienhuis (1983) Laugier et al. (1999), Mediterranean Philippart (1995), Netherlands Vermaat et al. (1987), Netherlands Vermaat and Verhagen (1996), Netherlands Plus et al. (2001), Mediterranean Pérez-Lloréns and Niell (1993), Spain	15 – 90	45	gC/m²
$Loss_N$	Shoot loss rate	0.042	Laugier et al. (1999)	0.01 - 0.09	0.01	-
d_{loss}	Day of year at which aging of leaves increases shoot loss rate		Esitmations from this study	240 - 300	260	Day of year
d_{grow}	Day of year at which recruitment starts		Estimations from this study	60 – 160	100	Day of year
k_{rs}	Fraction of growth that is allocated to below ground growth	0.21 * 0.19 * 0.3 * 0.17 * 0.4	Zharova et al. (2001) Verhagen and Nienhuis (1983) Bach (1993) McRoy (1974) Plus et al. (2003)	0.1 - 0.5	0.4	-
R_{upr}	Below ground biomass of plant lost due to uprooting	0.002	Zharova et al. (2001), based on Verhagen and Nienhuis (1983)	0.0005 - 0.0035	0.001	gC
$Loss_R$	Loss rate of below ground biomass	0.009	Zharova et al. (2001), based on Verhagen and Nienhuis (1983)	0.005 - 0.02	0.005	-

In the sensitivity analysis, only one of the parameters was varied in each simulation within the parameter scope described in Table A1, while the other parameters were kept constant. Figure A1 shows how the key variables, including the mean canopy height, shoot density, root biomass and the mean depth distribution of the seagrass biomass, respond to variation of the parameters.

Among the four key variables, the mean canopy height is the most sensitive to changes in the parameters. The growth and loss rate of the single leaf biomass has the biggest impact on the seagrass canopy height. A high growth rate leads to a higher canopy, and a higher loss rate leads to a lower canopy height. Other parameters that have a significant impact on the canopy height are the day of the year on which the growth of new shoots starts, the fraction of growth that is allocated to below ground growth, the optimal and maximum temperature for growth, the saturation irradiance and the day at which the loss of shoots starts.

The number of shoots is mostly influenced by changes to the loss rate of shoots. A low loss rate leads to a high number of shoots and vice versa. The number of shoots is also influenced by the shoot growth rate and the day at which the shoots start to grow.

The mean root biomass is influenced mostly by the root biomass loss rate and the shoot loss rate. A low loss rate leads to a higher root biomass and vice versa. The root biomass is also influenced by the shoot growth rate, and the growth rate of single shoot.

The depth distribution of the seagrass is influenced most by the day at which the growth of shoots starts, the loss rate of a single shoot, the saturation irradiance, the optimal temperature for growth, the growth rates of a single shoot, and the fraction of growth that is allocated to below ground growth.

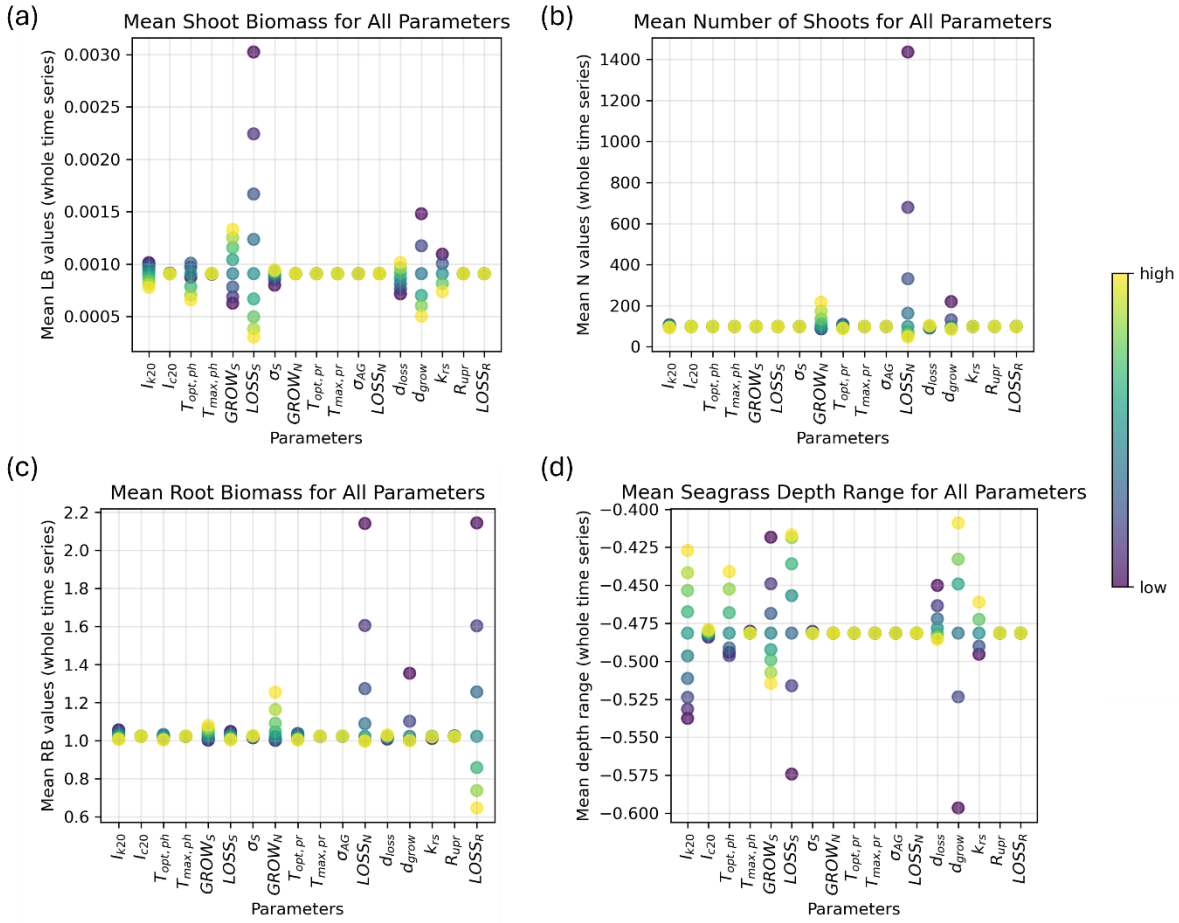

Figure A1: Impact of different parameter settings on seagrass growth, shown as the changes to mean (a) single shoot biomass, (b) number of shoots, (c) root biomass, and (d) mean depth of the distribution. Each parameter was changed over its scope defined in Table A1 while the other parameters were kept constant. For comparison purposes, the parameter values are marked high to low instead of the actual values. The range for each parameter is listed in Table A1.

Growth of seagrass in the model is driven by weekly averaged values of temperature, solar radiation, mean inundation time, and wind speed, which are calculated based on the simulation results of the hydrodynamic model.

The weekly averaged temperature represents the mean value for both water temperature when the seagrass meadow is inundated and air temperature otherwise:

$$\boldsymbol{T = avg(T_t)} \quad (\boldsymbol{A13})$$

The radiation is given by

$$\boldsymbol{I_{wc,n} = I_{n-1} \cdot \exp\left(-k_{e,n} \cdot \frac{d_{z,n}}{2}\right)}, \quad (\boldsymbol{A14})$$

$$\boldsymbol{I_n = I_{n-1} \cdot \exp(-k_{e,n} \cdot d_{z,n})}, \quad (\boldsymbol{A15})$$

where $I_{wc,n}$ is the radiation reaching the middle of layer n counted from the surface, I_{n-1} is the radiation reaching the bottom of the layer $n-1$, I_n is the radiation reaching the bottom of layer n and $d_{,nz}$ is the layer thickness of layer n. $k_{w,n}$ is the light extinction coefficient in laver n, which is calculated as

$$\boldsymbol{k_{e,n} = k_w + k_{sed} \cdot tsc_n}, \quad (\boldsymbol{A16})$$

where k_w is the background attenuation by water, k_{sed} is the light extinction coefficient by sediment turbidity and tsc_n is the sediment concentration in layer n. The radiation used as forcing is the average radiation reaching the middle of the bottom-most computational cell of the hydrodynamic model ($I_{wc,bot}$), which is the same as the incoming radiation at the surface for the timesteps at which the cell is dry:

$$\boldsymbol{I = avg(I_{wc,bot})}. \quad (\boldsymbol{A17})$$

The mean inundation time per tide in hours is calculated as

$$\boldsymbol{t_{dry} = \frac{t_{dry,week}}{n_{tides}}}, \quad (\boldsymbol{A18})$$

where $t_{dry,week}$ is the accumulative time when a computational cell is dry during a whole week, and n_{tides} is the number of tidal cycles in the same period.

The growth of the seagrass in the model is mostly driven by the temperature (figure A2a). During the main growth season, variations in solar radiation also noticeably influence the growth rate, especially during weeks with low solar radiation. For the biomass loss (figure A2b) the influence of both solar radiation and temperature is less prominent. The seasonality of the biomass loss is mostly driven by the seasonal loss terms summarized in the loss function f_{age}.

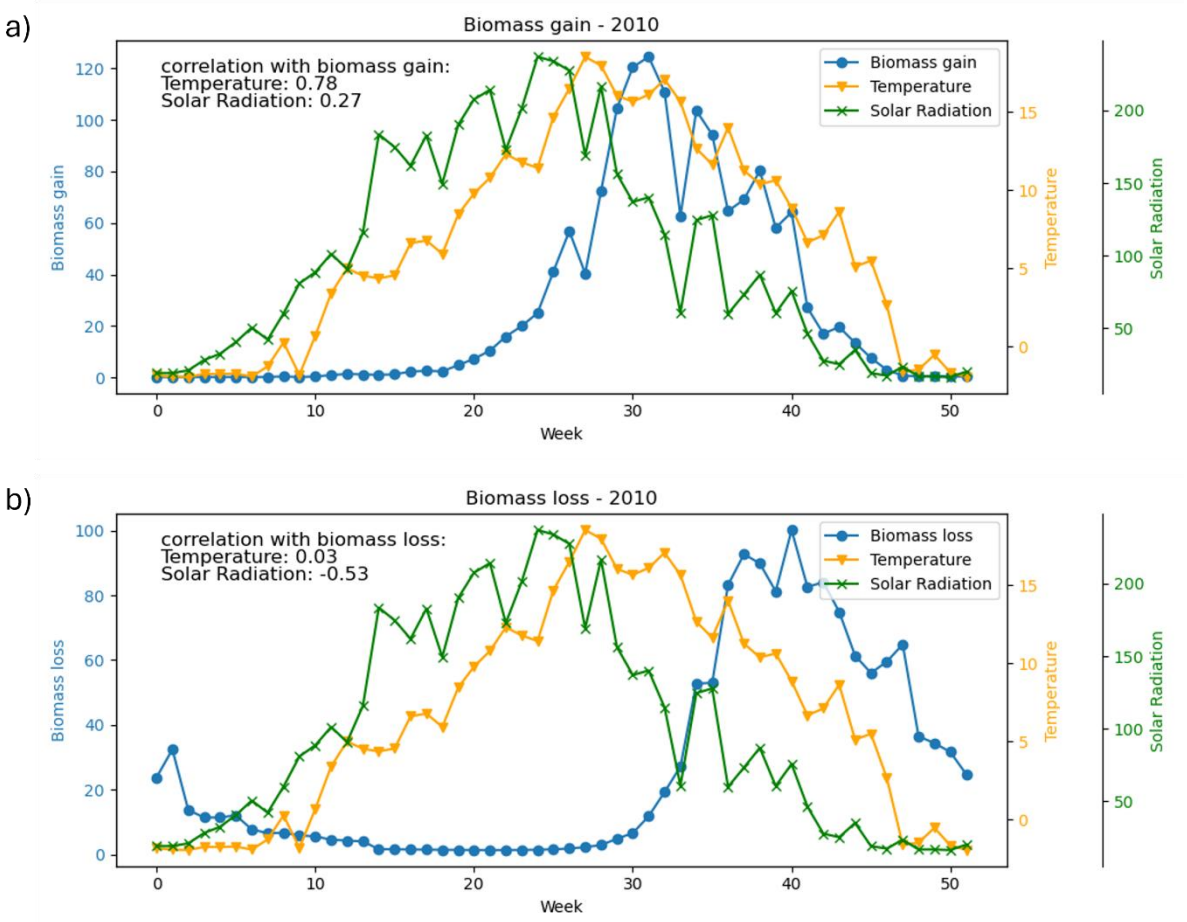

575 Figure A2: (a) Mean biomass gain together with weekly mean temperature and solar radiation used for forcing the seagrass model for 2010. (b) The same for biomass loss.

Appendix B – Sensitivity of the burial rate of POC to the choice of the conversion factor $f_{exp,AG}$

The conversion of above ground biomass to POC is determined by the conversion factor $f_{exp,AG}$. The factor is based on literature values (Duarte and Krause-Jensen, 2017; Zou et al., 2021). The burial rate of carbon inside the seagrass meadows
580 depends linearly on the amount of locally produced carbon, as can be seen in Fig. B1, where a reduction of the biomass that is converted to POC leads to an equally large reduction in POC that is buried in the meadow sediments.

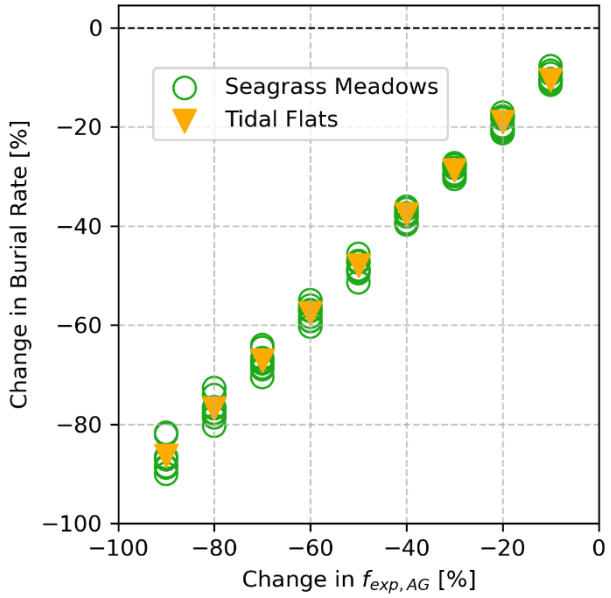

Figure B1: Relative change in burial rate of AG POC for tidal flats without seagrass cover in general and for several seagrass meadows, for different values of $f_{exp,AG}$, the fraction of seagrass biomass loss that is converted to POC.

Appendix C - Validation of the hydro-morphodynamic model

The performance of the hydro-morphodynamic model was evaluated through comparison of simulated and observed hydrodynamic and morphological variables (Mohr et al., 2025). Water levels and temperature were compared against available measurements at the tide gauges located inside the model domain, namely List Harbour (LIS) (Wasserstraßen- und Schifffahrtsamt Elbe-Norsee (WSA) am Standort Tönning), Havneby Harbour (HAV) and Vidaslusen (VIS) (Danmarks Meteorologiske Institut, 2024). The bathymetric changes were compared against the morphological changes in the easyGSH-DB digital terrain model (Sievers et al., 2020), averaged over 2010-2015 to mitigate effects of the spatially uneven measurement frequency.

The simulated water levels reproduced the observed dynamics, including the spring-neap tide tidal cycle and extreme high- and low-water events (Fig. C1a-b). The simulation slightly overestimates the tidal amplitudes.

The simulated water temperature is also consistent with observations (Fig. C1c), capturing the overall seasonality of temperature change, as well as short term variations. The simulation has a consistently 2°C lower temperature compared to the observations, which was considered during the tuning of the seagrass model.

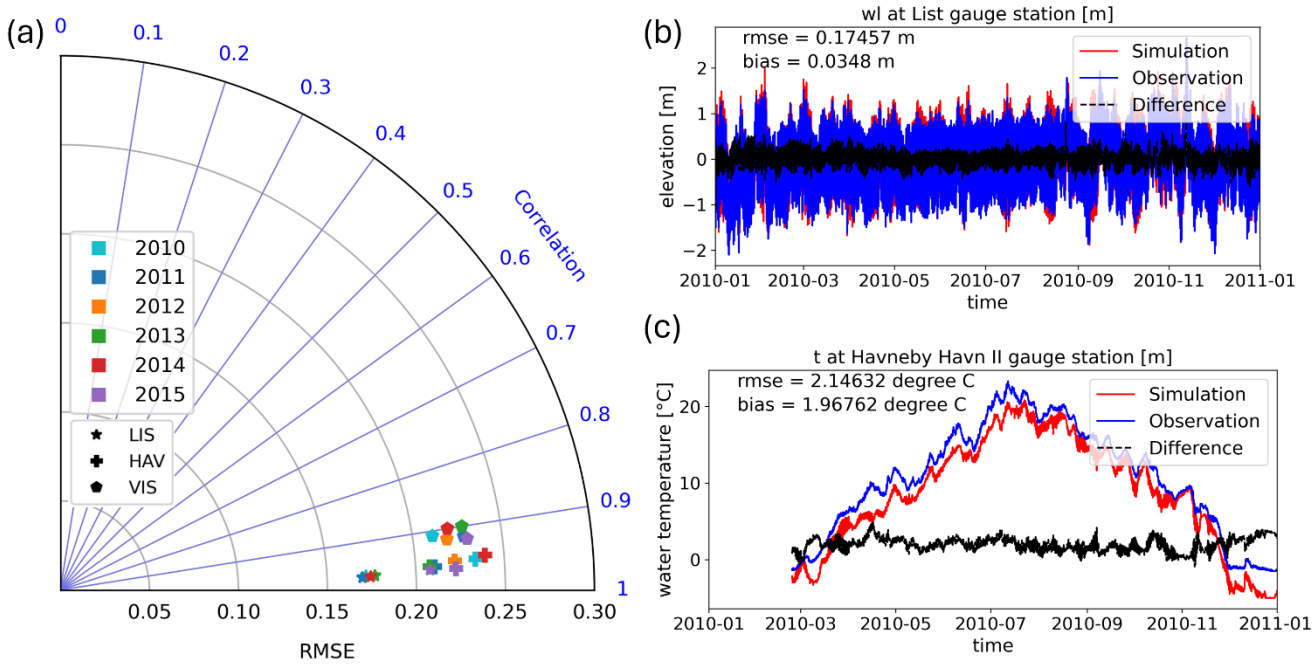

Figure C1: Comparison of observed and simulated water level and temperature: (a) the plot of correlation and RMSE includes the different stations for each year, using hourly data. The time series on the right show (b) the observed and simulated water level at List gauge station for 2010 and their difference and (c) the observed and simulated water temperature at Havneby Havn gauge station for 2010 and their difference, as an example for all simulated years. From Mohr et al. (2025)Mohr et al. (2025)Mohr et al. (2025).

Assessing the performance of the morphological model is complicated by artifacts and inconsistencies in the observational dataset, particularly in the intertidal zone where bathymetric measurements are difficult to obtain. It was further complicated by the asynchrony of surveys in the German and Danish part of the Sylt-Rømø Bay. Despite the noise in the resulting datasets, large scale morphological patterns are visible in the observations and are overall reproduced by the simulation (Figure C2). This applies to the channel migration detected in the observations: The two southern channels migrate to the north-east and the northern channel migrates to the southeast, which is reproduced by the simulation, though with differences in magnitude and spatial detail in the erosion and deposition patterns. Both simulation and observation show slight overall accumulation of sediments averaged over the tidal flats. Overall, the simulation captures the patterns of erosion and deposition in the bay, however with smoother spatial patterns due to limitations by the model grid resolution.

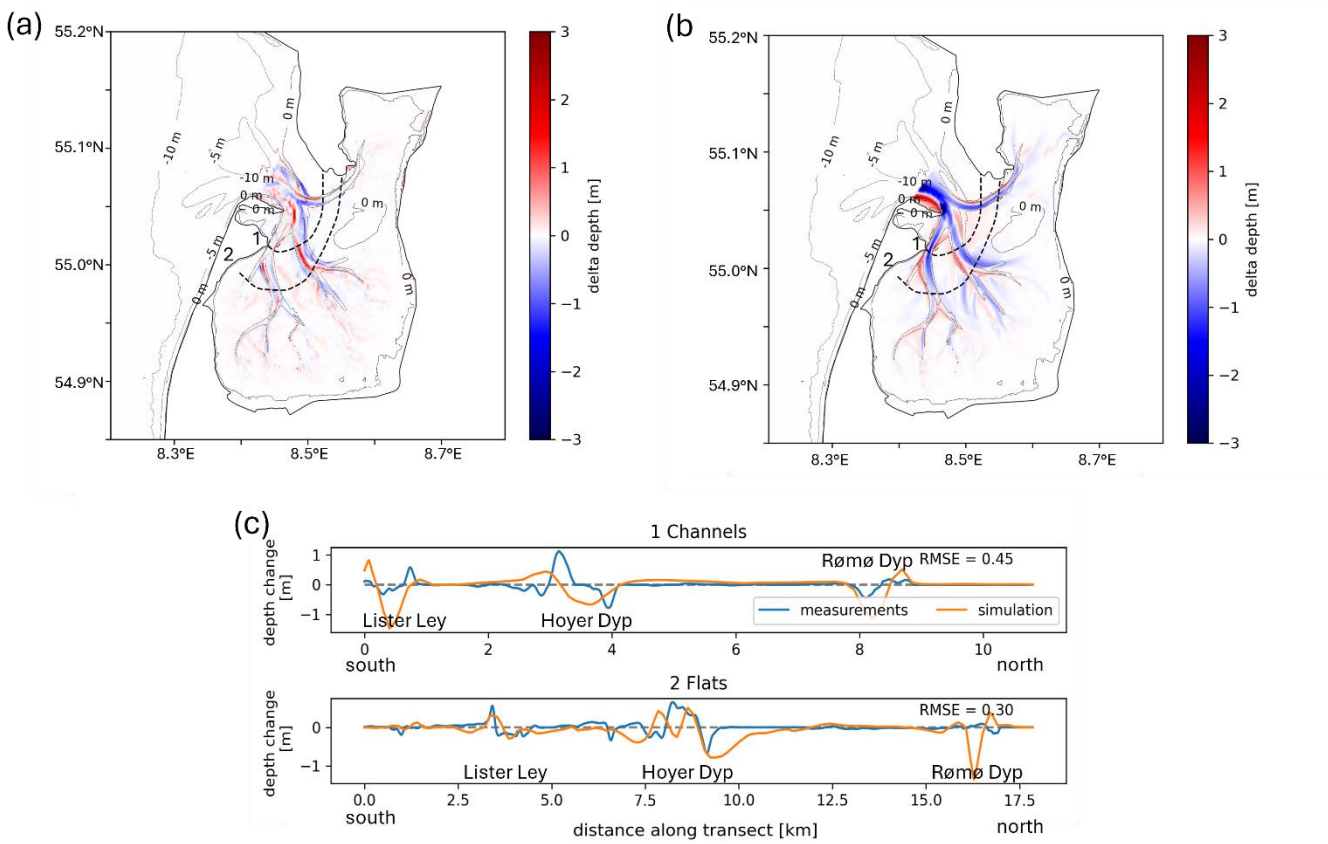

Figure C2: Depth changes in the Sylt-Rømø Bay for (a) observations and (b) simulation (SG-VO). Positive values show a decrease in depth, negative values an increase. The depth contours are at 0 m, -5 m and -10 m. The dashed lines show the location of transects across the inlet and the basin. The depth changes along two transects is shown in (c). The transects start at their southern end where the numbers are written. The values for both observed and simulated depth changes are the mean depth changes for the years 2010-2015. From Mohr et al. (2025).

Code Availability

This study used SCHISM v5.13 for the numerical simulations, which is available on GitHub (https://github.com/schism-dev/schism).

The code for the intertidal seagrass model SGINT is available at Mohr (2026b). The input parameter files for running the model, as well as the python codes, jupyter notebooks and auxiliary data used for analysing the model results can be found at Mohr (2026a).

Author Contributions

Conceptualization by VM, WZ. Model setup, evaluation and visualisation by VM. Result analysis by VM and WZ. Original draft by VM, review by CS, WZ. Funding acquisition by WZ, CS.

Competing Interests

The authors declare that they have no conflict of interest.

Acknowledgements

We would like to thank Dr. Tobias Dolch (AWI Wattenmeerstation Sylt) for providing the observational data from seagrass meadows in the Wadden Sea near the island of Sylt, and Lasse Ørsted Jensen for providing observational data for seagrass meadows in the Danish part of the bay.

Financial Support

This study is a contribution to the theme "A5: The Land-Ocean Transition Zone" of the Cluster of Excellence EXC 2037 'CLICCS -Climate, Climatic Change, and Society' -Project Number: 390683824 funded by the Deutsche Forschungsgemeinschaft (DFG, German Research Foundation) under Germany's Excellence Strategy. It is also supported by the Helmholtz research program in PoF IV "Changing Earth – Sustaining our Future" - "Topic 4: Coastal Transition Zones under Natural and Human Pressure". It is additionally supported by the Federal Ministry of Research, Technology and Space (BMFTR) through the project CoastalFutures II (Grant No.03F0980A) and the Helmholtz Imaging Platform project "AutoCoast-Automatic detection of coastline change and causal linkage with natural and human drivers" (ZT-IPF-4-048).

References

Abe, M., Hashimoto, N., Kurashima, A., and Maegawa, M.: Estimation of light requirement for the growth of *Zostera marina* in central Japan, Fisheries Science, 69, 890–895, https://doi.org/10.1046/j.1444-2906.2003.00704.x, 2003.

Alongi, D. M.: Seagrass Meadows, in: Blue Carbon: Coastal Sequestration for Climate Change Mitigation, Springer International Publishing, Cham, 37–51, https://doi.org/10.1007/978-3-319-91698-9_4, 2018.

do Amaral Camara Lima, M., Ward, R. D., and Joyce, C. B.: Carbon sequestration and geochronology in Southern England's seagrass meadows, Carbon Footprints, 2, https://doi.org/10.20517/cf.2023.08, 2023.

Arias Ortiz, A.: Carbon sequestration rates in coastal Blue Carbon ecosystems: a perspective on climate change mitigation, Ph.D. Thesis, Universitat Autònoma de Barcelona, Barcelona, 2019.

Arias-Ortiz, A., Lafratta, A., Colarusso, P., Fourqurean, J., Fu, C., Kennedy, H., Krause, J., Lavery, P., Leiva-Dueñas, C., Marba, N., Mateo, M., Mazarrasa, I., Poursanidis, D., Salinas, C., Serrano, O., Stankovic, M., Piñeiro, N., Werner, A., Wesselmann, M., Duarte, C. M., Garcia-Orellana, J., and Masque, P.: Seagrass sediment organic carbon burial rates are globally significant, https://doi.org/10.21203/rs.3.rs-8462059/v1, 6 January 2026.

Sedimentologische Parameter Modellgitterpunkte (Projekt AufMod) [Data set]: http://data.europa.eu/88u/dataset/2f6d8474-2915-4a64-af74-af3e922c4693, last access: 20 July 2023.

Azevedo, A., Lillebø, A. I., Lencart e Silva, J., and Dias, J. M.: Intertidal seagrass models: Insights towards the development and implementation of a desiccation module, Ecol. Modell., 354, 20–25, https://doi.org/10.1016/j.ecolmodel.2017.03.004, 2017.

Bach, H. K.: A dynamic model describing the seasonal variations in growth and the distribution of eelgrass (*Zostera marina* L.) I. Model theory, Ecol. Modell., 65, 31–50, https://doi.org/10.1016/0304-3800(93)90125-C, 1993.

de Beer, D., Wenzhöfer, F., Ferdelman, T. G., Boehme, S. E., Huettel, M., van Beusekom, J. E. E., Böttcher, M. E., Musat, N., and Dubilier, N.: Transport and mineralization rates in North Sea sandy intertidal sediments, Sylt-Rømø Basin, Wadden Sea, Limnol. Oceanogr., 50, 113–127, https://doi.org/10.4319/lo.2005.50.1.0113, 2005.

Berković, B., Cabaço, S., Barrio, J. M., Santos, R., Serrão, E. A., and Alberto, F.: Extending the life history of a clonal aquatic plant: Dispersal potential of sexual and asexual propagules of *Zostera noltii*, Aquat. Bot., 113, 123–129, https://doi.org/10.1016/j.aquabot.2013.10.007, 2014.

FES2014 Product [data set]: https://www.aviso.altimetry.fr/en/data/products/auxiliary-products/global-tide-fes/description-fes2014.html, last access: 6 July 2023.

Chang, Y.-E., Liao, C.-H., Hsieh, H.-H., Gradngay Abedneko, V., Hung, C.-C., and Lee, T.-M.: Lateral carbon export of macroalgae and seagrass from diverse habitats contributes particulate organic carbon in the deep sea of the Northern South China Sea, Mar. Pollut. Bull., 206, 116672, https://doi.org/10.1016/j.marpolbul.2024.116672, 2024.

Daewel, U. and Schrum, C.: Simulating long-term dynamics of the coupled North Sea and Baltic Sea ecosystem with ECOSMO II: Model description and validation, Journal of Marine Systems, 119–120, 30–49, https://doi.org/10.1016/j.jmarsys.2013.03.008, 2013.

Dahl, M., Deyanova, D., Gütschow, S., Asplund, M. E., Lyimo, L. D., Karamfilov, V., Santos, R., Björk, M., and Gullström, M.: Sediment Properties as Important Predictors of Carbon Storage in *Zostera marina* Meadows: A Comparison of Four European Areas, PLoS One, 11, e0167493, https://doi.org/10.1371/journal.pone.0167493, 2016.

Dahl, M., Gullström, M., Bernabeu, I., Serrano, O., Leiva-Dueñas, C., Linderholm, H. W., Asplund, M. E., Björk, M., Ou, T., Svensson, J. R., Andrén, E., Andrén, T., Bergman, S., Braun, S., Eklöf, A., Ežerinskis, Z., Garbaras, A., Hällberg, P., Löfgren, E., Kylander, M. E., Masqué, P., Šapolaitė, J., Smittenberg, R., and Mateo, M. A.: A 2,000-Year Record of Eelgrass (*Zostera marina* L.) Colonization Shows Substantial Gains in Blue Carbon Storage and Nutrient Retention, Global Biogeochem. Cycles, 38, https://doi.org/10.1029/2023GB008039, 2024.

Danmarks Meteorologiske Institut: Water level and water temperature observations [Data Set], https://www.dmi.dk/friedata/observationer/, 2024.

Datahuis Wadden: WMR - TMAP: Zoutmoeras [Dataset], https://datahuiswadden.openearth.nl/geonetwork/srv/dut/catalog.search#/metadata/D9N_OpZ7QmO-e35iM2HeQQ, 2023.

Dennison, W. C. and Alberte, R. S.: Photosynthetic responses of *Zostera marina* L. (Eelgrass) to in situ manipulations of light intensity, Oecologia, 55, 137–144, https://doi.org/10.1007/BF00384478, 1982.

Dolch, T., Buschbaum, C., and Reise, K.: Persisting intertidal seagrass beds in the northern Wadden Sea since the 1930s, J. Sea Res., 82, 134–141, https://doi.org/10.1016/j.seares.2012.04.007, 2013.

Dolch, T., Folmer, E. O., Frederiksen, M. S., Herlyn, M., van Katwijk, M. M., Kolbe, K., KrauseJensen, D., Schmedes, P., Westerbeek, E. P., and al., K. S. et: Seagrass, in: Wadden Sea Quality Status Report 2017, edited by: Kloepper, S., Baptist, M. J., Bostelmann, A., Busch, J. A., Buschbaum, C., Gutow, L., Janssen, G., Jensen, K., Jørgensen, H. P., Jong, F., Lüerßen, G., Schwarzer, K., Strempel, R., and Thieltges, D., Wilhelmshaven, Germany, 2017.

Duarte, C. M. and Cebrián, J.: The fate of marine autotrophic production, Limnol. Oceanogr., 41, 1758–1766, https://doi.org/10.4319/lo.1996.41.8.1758, 1996.

Duarte, C. M. and Krause-Jensen, D.: Export from Seagrass Meadows Contributes to Marine Carbon Sequestration, Front. Mar. Sci., 4, https://doi.org/10.3389/fmars.2017.00013, 2017.

Duarte, C. M., Middelburg, J. J., and Caraco, N.: Major role of marine vegetation on the oceanic carbon cycle, Biogeosciences, 2, 1–8, https://doi.org/10.5194/bg-2-1-2005, 2005.

Duarte, C. M., Marbà, N., Gacia, E., Fourqurean, J. W., Beggins, J., Barrón, C., and Apostolaki, E. T.: Seagrass community metabolism: Assessing the carbon sink capacity of seagrass meadows, Global Biogeochem. Cycles, 24, n/a-n/a, https://doi.org/10.1029/2010GB003793, 2010.

Duarte, C. M., Losada, I. J., Hendriks, I. E., Mazarrasa, I., and Marbà, N.: The role of coastal plant communities for climate change mitigation and adaptation, Nat. Clim. Chang., 3, 961–968, https://doi.org/10.1038/nclimate1970, 2013.

Fofonova, V., Androsov, A., Sander, L., Kuznetsov, I., Amorim, F., Hass, H. C., and Wiltshire, K. H.: Non-linear aspects of the tidal dynamics in the Sylt-Rømø Bight, south-eastern North Sea, Ocean Science, 15, 1761–1782, https://doi.org/10.5194/os-15-1761-2019, 2019.

Fonseca, M. S., Fisher, J. S., Zieman, J. C., and Thayer, G. W.: Influence of the seagrass, *Zostera marina* L., on current flow, Estuar. Coast. Shelf Sci., 15, 351–364, https://doi.org/10.1016/0272-7714(82)90046-4, 1982.

Greiner, J., Wilkinson, G., McGlathery, K., and Emery, K.: Sources of sediment carbon sequestered in restored seagrass meadows, Mar. Ecol. Prog. Ser., 551, 95–105, https://doi.org/10.3354/meps11722, 2016.

Harwell, M. C. and Orth, R. J.: Long-distance dispersal potential in a marine macrophyte, Ecology, 83, 3319–3330, https://doi.org/https://doi.org/10.1890/0012-9658(2002)083[3319:LDDPIA]2.0.CO;2, 2002.

Hommes, L.: Blue Carbon in the Wadden Sea: Organic Matter Built-up in *Zostera noltii* Seagrass Meadows and adjacent Tidal Flats in Schleswig-Holstein, German, Capstone Thesis, Leiden Universtiy, The Hague, 2023.

Hyndes, G. A., Berdan, E. L., Duarte, C., Dugan, J. E., Emery, K. A., Hambäck, P. A., Henderson, C. J., Hubbard, D. M., Lastra, M., Mateo, M. A., Olds, A., and Schlacher, T. A.: The role of inputs of marine wrack and carrion in sandy-beach ecosystems: a global review, Biological Reviews, 97, 2127–2161, https://doi.org/10.1111/brv.12886, 2022.

Lo Iacono, C., Mateo, M. A., Gràcia, E., Guasch, L., Carbonell, R., Serrano, L., Serrano, O., and Dañobeitia, J.: Very high-resolution seismo-acoustic imaging of seagrass meadows (Mediterranean Sea): Implications for carbon sink estimates, Geophys. Res. Lett., 35, L18601, https://doi.org/10.1029/2008GL034773, 2008.

Jacobs, R. P. W. M., Den Hartog, C., Braster, B. F., and Carriere, F. C.: Grazing of the seagrass *Zostera noltii* by birds at Terschelling (Dutch Wadden Sea), Aquat. Bot., 10, 241–259, https://doi.org/10.1016/0304-3770(81)90026-7, 1981.

Johannessen, S. C.: How can blue carbon burial in seagrass meadows increase long-term, net sequestration of carbon? A critical review, Environmental Research Letters, 17, 093004, https://doi.org/10.1088/1748-9326/ac8ab4, 2022.

Kappenberg, J., Fanger, H.-U., and Müller, A.: Currents and suspended particulate matter in tidal channels of the Sylt-Rømø basin, Senckenbergiana maritima, 29, 93–100, https://doi.org/10.1007/BF03043947, 1998.

Kennedy, H., Beggins, J., Duarte, C. M., Fourqurean, J. W., Holmer, M., Marbà, N., and Middelburg, J. J.: Seagrass sediments as a global carbon sink: Isotopic constraints, Global Biogeochem. Cycles, 24, https://doi.org/10.1029/2010GB003848, 2010.

Kennedy, H., Pagès, J. F., Lagomasino, D., Arias-Ortiz, A., Colarusso, P., Fourqurean, J. W., Githaiga, M. N., Howard, J. L., Krause-Jensen, D., Kuwae, T., Lavery, P. S., Macreadie, P. I., Marbà, N., Masqué, P., Mazarrasa, I., Miyajima, T., Serrano, O., and Duarte, C. M.: Species Traits and Geomorphic Setting as Drivers of Global Soil Carbon Stocks in Seagrass Meadows, Global Biogeochem. Cycles, 36, https://doi.org/10.1029/2022GB007481, 2022.

Kloepper, S., Baptist, M. J., Bostelmann, A., Busch, J. A., Buschbaum, C., Gutow, L., Janssen, G., Jensen, K., Jørgensen, H. P., Jong, F., Lüerßen, G., Schwarzer, K., Strempel, R., and Thieltges, D. (Eds.): Wadden Sea Quality Status Report 2017, Wilhelmshaven, Germany, 2017.

Kohlmeier, D.: Light acclimation in intertidal seagrass: spatial and diurnal variations and the role of suspended sediments, Phd Thesis, Universität Bremen, Bremen, 2016.

Kombiadou, K., Ganthy, F., Verney, R., Plus, M., and Sottolichio, A.: Modelling the effects of *Zostera noltei* meadows on sediment dynamics: application to the Arcachon lagoon, Ocean Dyn., 64, 1499–1516, https://doi.org/10.1007/s10236-014-0754-1, 2014.

Konyssova, G., Sidorenko, V., Androsov, A., Sander, L., Danilov, S., Rubinetti, S., Burchard, H., Winter, C., and Wiltshire, K. H.: Changes in tidal dynamics in response to sea level rise in the Sylt-Rømø Bight (Wadden Sea), Ocean Dyn., 75, 43, https://doi.org/10.1007/s10236-025-01688-1, 2025.

Koplin, J., Peter, C., Bischof, K., Böttcher, M. E., Kuhn, A., Logemann, E., Dolch, T., Henkel, S., McCarthy, D., Mueller, P., Morys, C., Pineda-Metz, S. E. A., Reents, S., Reusch, T. B. H., Röschel, L., Rupprecht, F., Stevenson, A., Wiltshire, K. H., Zimmer, M., and Pogoda, B.: Blue Carbon potential in Germany: Status and future development, Estuar. Coast. Shelf Sci., 323, 109354, https://doi.org/10.1016/j.ecss.2025.109354, 2025.

Krumhansl, K. A., Lee, K. C., Ma, Y., Wu, Y., Baker, T. H. A., Wong, M. C., Azetsu-Scott, K., and Gentleman, W. C.: Pathways of blue carbon export from kelp and seagrass beds along the Atlantic coast of Nova Scotia, Sci. Adv., 11, https://doi.org/https://doi.org/10.1126/sciadv.adw1952, 2015.

de la Vega, C., Horn, S., Baird, D., Hines, D., Borrett, S., Jensen, L. F., Schwemmer, P., Asmus, R., Siebert, U., and Asmus, H.: Seasonal dynamics and functioning of the Sylt-Rømø Bight, northern Wadden Sea, Estuar. Coast. Shelf Sci., 203, 100–118, https://doi.org/10.1016/j.ecss.2018.01.021, 2018.

Laugier, T., Rigollet, V., and Casabianca, M.-L.: Seasonal dynamics in mixed eelgrass beds, *Zostera marina* L. and *Z. noltii* Hornem., in a Mediterranean coastal lagoon (Thau lagoon, France), Aquat. Bot., 63, 51–69, https://doi.org/10.1016/S0304-3770(98)00105-3, 1999.

Lavery, P. S., Mateo, M.-Á., Serrano, O., and Rozaimi, M.: Variability in the Carbon Storage of Seagrass Habitats and Its Implications for Global Estimates of Blue Carbon Ecosystem Service, PLoS One, 8, e73748, https://doi.org/10.1371/journal.pone.0073748, 2013.

Lettmann, K. A., Wolff, J.-O., and Badewien, T. H.: Modeling the impact of wind and waves on suspended particulate matter fluxes in the East Frisian Wadden Sea (southern North Sea), Ocean Dyn., 59, 239–262, https://doi.org/10.1007/s10236-009-0194-5, 2009.

Leuschner, C. and Rees, U.: CO2 gas exchange of two intertidal seagrass species, *Zostera marina* L. and *Zostera noltii* Hornem., during emersion, Aquat. Bot., 45, 53–62, https://doi.org/10.1016/0304-3770(93)90052-X, 1993.

LKN.SH Nationalparkverwaltung: Seegras-Vorkommen: Makrophyten-Monitoring im Schleswig-Holsteinisches Wattenmeer ab 1994 (UIG) [dataset], https://umweltportal.schleswig-holstein.de/trefferanzeige?docuuid=00100e9d-7838-4563-9dd7-2570b0d932cb, 2024.

Lovelock, C. E. and Duarte, C. M.: Dimensions of Blue Carbon and emerging perspectives, Biol. Lett., 15, 20180781, https://doi.org/10.1098/rsbl.2018.0781, 2019.

Macreadie, P. I., Costa, M. D. P., Atwood, T. B., Friess, D. A., Kelleway, J. J., Kennedy, H., Lovelock, C. E., Serrano, O., and Duarte, C. M.: Blue carbon as a natural climate solution, Nat. Rev. Earth Environ., 2, 826–839, https://doi.org/10.1038/s43017-021-00224-1, 2021.

Marsh, J. A., Dennison, W. C., and Alberte, R. S.: Effects of temperature on photosynthesis and respiration in eelgrass (*Zostera marina* L.), J. Exp. Mar. Biol. Ecol., 101, 257–267, https://doi.org/10.1016/0022-0981(86)90267-4, 1986.

Martins, M., de los Santos, C. B., Masqué, P., Carrasco, A. R., Veiga-Pires, C., and Santos, R.: Carbon and Nitrogen Stocks and Burial Rates in Intertidal Vegetated Habitats of a Mesotidal Coastal Lagoon, Ecosystems, 25, 372–386, https://doi.org/10.1007/s10021-021-00660-6, 2022.

Massa, S. I., Arnaud-Haond, S., Pearson, G. A., and Serrão, E. A.: Temperature tolerance and survival of intertidal populations of the seagrass *Zostera noltii* (Hornemann) in Southern Europe (Ria Formosa, Portugal), Hydrobiologia, 619, 195–201, https://doi.org/10.1007/s10750-008-9609-4, 2009.

Mateo, M. A.: Beach-Cast *Cymodocea nodosa* Along the Shore of a Semienclosed Bay: Sampling and Elements to Assess Its Ecological Implications, J. Coast. Res., 262, 283–291, https://doi.org/10.2112/08-1100.1, 2010.

Mazarrasa, I., Marbà, N., Lovelock, C. E., Serrano, O., Lavery, P. S., Fourqurean, J. W., Kennedy, H., Mateo, M. A., Krause-Jensen, D., Steven, A. D. L., and Duarte, C. M.: Seagrass meadows as a globally significant carbonate reservoir, Biogeosciences, 12, 4993–5003, https://doi.org/10.5194/bg-12-4993-2015, 2015.

Mcleod, E., Chmura, G. L., Bouillon, S., Salm, R., Björk, M., Duarte, C. M., Lovelock, C. E., Schlesinger, W. H., and Silliman, B. R.: A blueprint for blue carbon: toward an improved understanding of the role of vegetated coastal habitats in sequestering CO2, Front. Ecol. Environ., 9, 552–560, https://doi.org/10.1890/110004, 2011.

McRoy, C. P.: Seagrass productivity: Carbon uptake experiments in eelgrass, *Zostera marina*, Aquaculture, 4, 131–137, https://doi.org/10.1016/0044-8486(74)90028-3, 1974.

Mengis, N., Kalhori, A., Simon, S., Harpprecht, C., Baetcke, L., Prats-Salvado, E., Schmidt-Hattenberger, C., Stevenson, A., Dold, C., El Zohbi, J., Borchers, M., Thrän, D., Korte, K., Gawel, E., Dolch, T., Heß, D., Yeates, C., Thoni, T., Markus, T., Schill, E., Xiao, M., Köhnke, F., Oschlies, A., Förster, J., Görl, K., Dornheim, M., Brinkmann, T., Beck, S., Bruhn, D., Li, Z., Steuri, B., Herbst, M., Sachs, T., Monnerie, N., Pregger, T., Jacob, D., and Dittmeyer, R.: Net-Zero CO_2 Germany—A Retrospect From the Year 2050, Earths Future, 10, https://doi.org/10.1029/2021EF002324, 2022.

Mohr, V.: VeroM96/PythonScripts_SR_SeagrassCarbon: Plotting scripts for first version of Manuscript [code], https://doi.org/10.5281/zenodo.18435872, January 2026a.

Mohr, V.: VeroM96/SGINT: SGINT for SCHISM v5.13 [code], https://doi.org/10.5281/zenodo.18435883, January 2026b.

Mohr, V., Zhang, W., Dolch, T., and Schrum, C.: The Importance of Seasonality in Seagrass Properties for Coastal Hydro-Morphodynamics—A Case Study in a Wadden Sea Basin, J. Geophys. Res. Earth Surf., 130, https://doi.org/10.1029/2025JF008331, 2025.

Mueller, P., Ladiges, N., Jack, A., Schmiedl, G., Kutzbach, L., Jensen, K., and Nolte, S.: Assessing the long-term carbon-sequestration potential of the semi-natural salt marshes in the European Wadden Sea, Ecosphere, 10, https://doi.org/10.1002/ecs2.2556, 2019.

Olesen, B. and Sand-Jensen, K.: Seasonal acclimatization of eelgrass *Zostera marina* growth to light, Mar. Ecol. Prog. Ser., 94, 91–99, https://doi.org/10.3354/meps094091, 1993.

Oppelt, N., Uhl, F., and Martius, J.: Erstellung von GIS-Karten zur Kohlenstoffspeicherung an der deutschen Nordseeküste - Methodische Projektdokumentation, 1–13 pp., 2024.

Oreska, M. P. J., Wilkinson, G. M., McGlathery, K. J., Bost, M., and McKee, B. A.: Non-seagrass carbon contributions to seagrass sediment blue carbon, Limnol. Oceanogr., 63, https://doi.org/10.1002/lno.10718, 2018.

Pan, Y. and Holmer, M.: Seagrass and macroalgae on shores: unraveling the decomposition of beach wrack on Danish coasts, Estuar. Coast. Shelf Sci., 324, 109473, https://doi.org/10.1016/j.ecss.2025.109473, 2025.

Pejrup, M., Larsen, M., and Edelvang, K.: A fine-grained sediment budget for the Sylt-Rømø tidal basin, Helgoländer Meeresuntersuchungen, 51, 253–268, https://doi.org/10.1007/BF02908714, 1997.

Peralta, G., Pérez-Lloréns, J. L., Hernández, I., Brun, F., Vergara, J. J., Bartual, A., Gálvez, J. A., and García, C. M.: Morphological and physiological differences between two morphotypes of *Zostera noltii* Hornem. from the south-western Iberian Peninsula, Helgol. Mar. Res., 54, 80–86, https://doi.org/10.1007/s101520050005, 2000.

Peralta, G., Pérez-Lloréns, J. L., Hernández, I., and Vergara, J. J.: Effects of light availability on growth, architecture and nutrient content of the seagrass *Zostera noltii* Hornem, J. Exp. Mar. Biol. Ecol., 269, 9–26, https://doi.org/10.1016/S0022-0981(01)00393-8, 2002.

Pérez, M.: Fanerógamas marinas en sistemas estuáricos: Producción, factores limitantes y algunos aspectos del ciclo de nutrientes, PhD Thesis, University of Barcelona, Barcelona, 244 pp., 1989.

Pérez-Lloréns, J. L. and Niell, F. X.: Seasonal dynamics of biomass and nutrient content in the intertidal seagrass *Zostera noltii* Hornem. from Palmones River estuary, Spain, Aquat. Bot., 46, 49–66, https://doi.org/10.1016/0304-3770(93)90064-4, 1993.

Philippart, C. J. M.: Seasonal variation in growth and biomass of an intertidal *Zostera noltii* stand in the Dutch Wadden Sea, Netherlands Journal of Sea Research, 33, 205–218, https://doi.org/10.1016/0077-7579(95)90007-1, 1995.

Piñeiro-Juncal, N., Mateo, M. Á., Leiva-Dueñas, C., Serrano, E., Inostroza, K., Soler, M., Apostolaki, E. T., Lavery, P., Duarte, C. M., Lafratta, A., and Serrano, O.: Soil organic carbon depth profiles and centennial and millennial decay rates in tidal marsh, mangrove and seagrass blue carbon ecosystems, Commun. Earth Environ., 6, 504, https://doi.org/10.1038/s43247-025-02390-2, 2025.

Pinto, L., Fortunato, A. B., Zhang, Y., Oliveira, A., and Sancho, F. E. P.: Development and validation of a three-dimensional morphodynamic modelling system for non-cohesive sediments, Ocean Model. (Oxf)., 57–58, 1–14, https://doi.org/10.1016/j.ocemod.2012.08.005, 2012.

Plus, M., Deslous-Paoli, J.-M., Auby, I., and Dagault, F.: Factors influencing primary production of seagrass beds (*Zostera noltii* Hornem.) in the Thau lagoon (French Mediterranean coast), J. Exp. Mar. Biol. Ecol., 259, 63–84, https://doi.org/10.1016/S0022-0981(01)00223-4, 2001.

Plus, M., Chapelle, A., Ménesguen, A., Deslous-Paoli, J.-M., and Auby, I.: Modelling seasonal dynamics of biomasses and nitrogen contents in a seagrass meadow (*Zostera noltii* Hornem.): application to the Thau lagoon (French Mediterranean coast), Ecol. Modell., 161, 213–238, https://doi.org/10.1016/S0304-3800(02)00350-2, 2003.

Postlethwaite, V. R., McGowan, A. E., Kohfeld, K. E., Robinson, C. L. K., and Pellatt, M. G.: Low blue carbon storage in eelgrass (*Zostera marina*) meadows on the Pacific Coast of Canada, PLoS One, 13, e0198348, https://doi.org/10.1371/journal.pone.0198348, 2018.

Potouroglou, M.: Assessing the role of intertidal seagrasses as coastal carbon sinks in Scotland, PhD Thesis, Edinburgh Napier University, Edinburgh, 2017.

Prentice, C., Poppe, K. L., Lutz, M., Murray, E., Stephens, T. A., Spooner, A., Hessing-Lewis, M., Sanders-Smith, R., Rybczyk, J. M., Apple, J., Short, F. T., Gaeckle, J., Helms, A., Mattson, C., Raymond, W. W., and Klinger, T.: A Synthesis of Blue Carbon Stocks, Sources, and Accumulation Rates in Eelgrass (*Zostera marina*) Meadows in the Northeast Pacific, Global Biogeochem. Cycles, 34, https://doi.org/10.1029/2019GB006345, 2020.

Rasmussen, E.: Systematics and ecology of the Isefjord marine fauna (Denmark), Ophelia, 11, 1–507, https://doi.org/10.1080/00785326.1973.10430115, 1973.

Reise, K.: Coastal change in a tidal backbarrier basin of the northern Wadden Sea: Are tidal flats fading away?, Senckenbergiana maritima, 29, 121–127, https://doi.org/10.1007/BF03043950, 1998.

Ricart, A. M., York, P. H., Rasheed, M. A., Pérez, M., Romero, J., Bryant, C. V, and Macreadie, P. I.: Variability of sedimentary organic carbon in patchy seagrass landscapes, Mar. Pollut. Bull., 100, 476–482, https://doi.org/10.1016/j.marpolbul.2015.09.032, 2015.

Ricart, A. M., York, P. H., Bryant, C. V., Rasheed, M. A., Ierodiaconou, D., and Macreadie, P. I.: High variability of Blue Carbon storage in seagrass meadows at the estuary scale, Sci. Rep., 10, 5865, https://doi.org/10.1038/s41598-020-62639-y, 2020.

Röhr, M. E., Boström, C., Canal-Vergés, P., and Holmer, M.: Blue carbon stocks in Baltic Sea eelgrass (*Zostera marina*) meadows, Biogeosciences, 13, 6139–6153, https://doi.org/10.5194/bg-13-6139-2016, 2016.

Röhr, M. E., Holmer, M., Baum, J. K., Björk, M., Boyer, K., Chin, D., Chalifour, L., Cimon, S., Cusson, M., Dahl, M., Deyanova, D., Duffy, J. E., Eklöf, J. S., Geyer, J. K., Griffin, J. N., Gullström, M., Hereu, C. M., Hori, M., Hovel, K. A., Hughes, A. R., Jorgensen, P., Kiriakopolos, S., Moksnes, P., Nakaoka, M., O'Connor, M. I., Peterson, B., Reiss, K., Reynolds, P. L., Rossi, F., Ruesink, J., Santos, R., Stachowicz, J. J., Tomas, F., Lee, K., Unsworth, R. K. F., and Boström, C.: Blue Carbon Storage Capacity of Temperate Eelgrass (*Zostera marina*) Meadows, Global Biogeochem. Cycles, 32, 1457–1475, https://doi.org/10.1029/2018GB005941, 2018.

Schaefer, R., Colarusso, P., Simpson, J. C., Novak, A., and Nepf, H.: Proximity to inlet channel drives spatial variation in sediment organic carbon across a lagoonal seagrass meadow, Science of The Total Environment, 177022, https://doi.org/10.1016/j.scitotenv.2024.177022, 2024.

Schaefer, R., Colarusso, P., Simpson, J. C., Novak, A., and Nepf, H.: Continual migration of patches within a Massachusetts seagrass meadow limits carbon accretion and storage, Commun. Earth Environ., 6, 129, https://doi.org/10.1038/s43247-025-02049-y, 2025.

Schanz, A. and Asmus, H.: Impact of hydrodynamics on development and morphology of intertidal seagrasses in the Wadden Sea, Mar. Ecol. Prog. Ser., 261, 123–134, https://doi.org/10.3354/meps261123, 2003.

Schildt, N.: The Carbon Storage Potential of Seagrass Meadows in the Eastern Wadden Sea and its possible Environmental Drivers, Master's thesis, Universität Bremen, Bremen, 2025.

Serrano, O., Lavery, P. S., Duarte, C. M., Kendrick, G. A., Calafat, A., York, P. H., Steven, A., and Macreadie, P. I.: Can mud (silt and clay) concentration be used to predict soil organic carbon content within seagrass ecosystems?, Biogeosciences, 13, 4915–4926, https://doi.org/10.5194/bg-13-4915-2016, 2016.

Sevdari, K. and Marmullaku, D.: Shapefile of European countries [Dataset], https://doi.org/10.11583/DTU.23686383, 2023.

Sievers, J., Rubel, M., and Milbradt, P.: EasyGSH-DB: Themengebiet - Sedimentologie [Data set], https://doi.org/https://doi.org/10.48437/02.2020.K2.7000.0005, 2020.

Suykerbuyk, W., Govers, L. L., van Oven, W. G., Giesen, K., Giesen, W. B. J. T., de Jong, D. J., Bouma, T. J., and van Katwijk, M. M.: Living in the intertidal: desiccation and shading reduce seagrass growth, but high salinity or population of origin have no additional effect, PeerJ, 6, e5234, https://doi.org/10.7717/peerj.5234, 2018.

Trevathan-Tackett, S. M., Jeffries, T. C., Macreadie, P. I., Manojlovic, B., and Ralph, P.: Long-term decomposition captures key steps in microbial breakdown of seagrass litter, Science of The Total Environment, 705, 135806, https://doi.org/10.1016/j.scitotenv.2019.135806, 2020.

Umlauf, L. and Burchard, H.: Second-order turbulence closure models for geophysical boundary layers. A review of recent work, Cont. Shelf Res., 25, 795–827, https://doi.org/10.1016/j.csr.2004.08.004, 2005.

Vennell, R., Scheel, M., Weppe, S., Knight, B., and Smeaton, M.: Fast lagrangian particle tracking in unstructured ocean model grids, Ocean Dyn., 71, 423–437, https://doi.org/10.1007/s10236-020-01436-7, 2021.

Verhagen, J. H. G. and Nienhuis, P. H.: A Simulation Model of Production, Seasonal Changes in Biomass and Distribution of Eelgrass (*Zostera marina*) in Lake Grevelingen, Mar. Ecol. Prog. Ser., 10, 187–195, https://doi.org/10.3354/meps010187, 1983.

Vermaat, J. E. and Verhagen, F. C. A.: Seasonal variation in the intertidal seagrass *Zostera noltii* Hornem.: coupling demographic and physiological patterns, Aquat. Bot., 52, 259–281, https://doi.org/10.1016/0304-3770(95)00510-2, 1996.

Vermaat, J. E., Hootsmans, M. J. M., and Nienhuis, P. H.: Seasonal dynamics and leaf growth of *Zostera noltii* Hornem., A perennial intertidal seagrass, Aquat. Bot., 28, 287–299, https://doi.org/10.1016/0304-3770(87)90006-4, 1987.

Voinov, A. A. and Akhremenkov, A. A.: Simulation modeling system for aquatic bodies, Ecol. Modell., 52, 181–205, https://doi.org/10.1016/0304-3800(90)90015-9, 1990.

Ward, E. A., Reynolds, S. E., Leng, M. J., Lacey, J. H., Cerasuolo, M., Paxton, B., Ragazzola, F., and Preston, J.: Mixed provenance of organic carbon in Northeast Atlantic temperate intertidal seagrass sediments, Sci. Rep., 15, 27892, https://doi.org/10.1038/s41598-025-12223-z, 2025.

Wasserstand (Ganglinie) Mess-Station Helgoland Binnenhafen [Data Set]: www.kuestendaten.de, last access: 18 January 2024.

Weatherall, E. J., Jackson, E. L., Hendry, R. A., and Campbell, M. L.: Quantifying the dispersal potential of seagrass vegetative fragments: A comparison of multiple subtropical species, Estuar. Coast. Shelf Sci., 169, 207–215, https://doi.org/10.1016/j.ecss.2015.11.026, 2016.

Zeiler, M. ;, Milbradt, P. ;, Plüß, A. ;, and Valerius, J.: Modelling Large Scale Sediment Transport in the German Bight (North Sea), Die Küste, 369–392, 2014.

Zhang, Y. J., Ye, F., Stanev, E. V, and Grashorn, S.: Seamless cross-scale modeling with SCHISM, Ocean Model. (Oxf)., 102, 64–81, https://doi.org/10.1016/j.ocemod.2016.05.002, 2016.

Zhang, Y. J., Gerdts, N., Ateljevich, E., and Nam, K.: Simulating vegetation effects on flows in 3D using an unstructured grid model: model development and validation, Ocean Dyn., 70, 213–230, https://doi.org/10.1007/s10236-019-01333-8, 2020.

Zharova, N., Sfriso, A., Voinov, A., and Pavoni, B.: A simulation model for the annual fluctuation of *Zostera marina* biomass in the Venice lagoon, Aquat. Bot., 70, 135–150, https://doi.org/10.1016/S0304-3770(01)00151-6, 2001.

Zimmermann, R. C., Smith, R. D., and Alberte, R. S.: Is growth of eelgrass nitrogen limited? A numerical simulation of the effects of light and nitrogen on the growth dynamics of *Zostera marina*, Mar. Ecol. Prog. Ser., 41, 167–176, 1987.

Zou, Y.-F., Chen, K.-Y., and Lin, H.-J.: Significance of belowground production to the long-term carbon sequestration of intertidal seagrass beds, Science of The Total Environment, 800, 149579, https://doi.org/10.1016/j.scitotenv.2021.149579, 2021.